## Title

RADIATION SHIELDING FOR HIGH ENERGY MUONS: THE CASE OF A CYLINDRICALLY SYMMETRICAL SHIELD AND NO MAGNETIC FIELDS



## Authors

Keefe, D.
Noble, C. M.

## Publication Date

1968-03-01

UCRL-18117
cy. 2



# University of California

# Ernest O. Lawrence Radiation Laboratory

RADIATION SHIELDING FOR HIGH ENERGY MUONS:
THE CASE OF A CYLINDRICALLY SYMMETRICAL SHIELD
AND NO MAGNETIC FIELDS

D. Keefe and C. M. Noble

March 1968

## DISCLAIMER

UCRL-18117
UC-34 Physics
TID-4500 (51st Ed.)

UNIVERSITY OF CALIFORNIA

Lawrence Radiation Laboratory
Berkeley, California

AEC Contract No. W-7405-eng-48

# RADIATION SHIELDING FOR HIGH ENERGY MUONS: THE CASE OF A CYLINDRICALLY SYMMETRICAL SHIELD AND NO MAGNETIC FIELDS

D. Keefe and C. M. Noble

March 1968

Printed in the United States of America
Available from
Clearinghouse for Federal Scientific and Technical Information
National Bureau of Standards, U. S. Department of Commerce
Springfield, Virginia 22151
Price: Printed Copy $3.00; Microfiche $0.65

# RADIATION SHIELDING FOR HIGH ENERGY MUONS: THE CASE OF A CYLINDRICALLY SYMMETRICAL SHIELD AND NO MAGNETIC FIELDS

D. Keefe and C. M. Noble

Lawrence Radiation Laboratory
University of California
Berkeley, California

March 1968

## Abstract

At proton accelerators with energies of tens of GeV and more, the shielding problems are dominated by the requirement of reducing the flux of muons to tolerable levels. This is especially true for accelerators making extensive use of extracted proton beams. We present a technique for calculating the profile of the radiation shield for muons for a number of practical situations of interest, viz., beam loss in an internal target area, beam loss during transport of the extracted proton beam down a long narrow pipe, and the case in which the extracted proton beam is dumped in a backstop. Results obtained from a computer program are presented graphically for different possible shield materials--heavy concrete, iron, lead, and depleted uranium. The results span four orders of magnitude in muon flux normalized to the rate of interacting protons, so that one can obtain useful results by interpolation for a wide variety of beam loss and desired shielding situations. The primary proton energies used in the calculations--25, 70, 200, and 300 GeV--will be recognized as corresponding to the energies of proton accelerators at present either operating or under design.

# RADIATION SHIELDING FOR HIGH ENERGY MUONS: THE CASE OF A CYLINDRICALLY SYMMETRICAL SHIELD AND NO MAGNETIC FIELDS

D. Keefe and C. M. Noble

Lawrence Radiation Laboratory
University of California
Berkeley, California

March 1968

## 1. Statement of the problem; definitions

A previous report[1] discussed the main factors involved in shielding against muons, and treated in a crude way the calculation of the extent of such shields in both the absence and presence of magnetic fields. Although the approach described there involved many approximations, it did serve as a useful basis for comparing the volume of shielding needed, for different assumptions about the nature of the materials. A program to refine these calculations has been in progress in connection with the shielding requirements for the 200 GeV accelerator, and results are reported here for the case in which no magnetic fields are involved close to the origin of the muons.

### 1.1 Geometry

We are concerned with two geometrical configurations that are of practical interest. First there is the case of a target placed in a proton beam passing along a cylindrical cavity surrounded by a thick cylindrical shield (see Fig. 1). This could correspond to targeting in a straight section of the extracted beam or in a field-free region of a Collins straight section of the internal beam. Alternatively, it could correspond to beam loss in the vacuum chamber, transport magnets, or

collimators in the extracted beam, provided a suitable line integral were included in the calculation. Second, there is the case of the backstop, where the proton beam strikes a solid block of material, and we need to know the extent of the block of material required to constitute a biologically safe shield against muons. Within certain approximations the backstop problem can be treated as a special--and simpler--case of the cavity problem, and we therefore concentrate the discussion on the first case.

1.2 Variables

Certain of the basic variables are shown in Fig. 1. Protons are assumed to strike a target on the axis. Pions are considered to be produced at angle $\theta$ with respect to the forward direction and, if they decay to muons, this angle, to a very good approximation, is preserved. (The maximum angle in $\pi$-$\mu$ decay is $0.04/P_\pi$, where $P_\pi$ is in GeV/c, which is much less than the typical angle, $\theta$, of production for the pions.) The contribution due to kaons is ignored here and is believed, from preliminary calculations, to be a small, almost constant percentage correction to the results obtained by considering pions alone. The energy of the pions is also assumed to be high enough that the distinction between momentum and energy can be neglected. We will consider the flux at a radius $r$ in the shield at a distance $L$ from the target. For a particle traveling in a straight line from the target the distance traversed through solid material is denoted by $S$. Thus, for energy-loss calculations, $S$ is the relevant quantity, while for inverse-square-law attenuation, $L$ is the important variable. The cavity radius $d$ will be taken as about 0.15 m for the external beam

(close-packed shielding) and about 2 m for the internal beam (man-sized tunnel). The first case will be denoted "cavity," the second "tunnel" in the presentation of the results. The approximation that $\theta$ is small enough to set $\sin\theta = \tan\theta = \theta$ and $\cos\theta = 1$ will be maintained throughout, so that the profile of the shield will not be correctly calculated within a few meters of the source.

1.3 Materials

The pertinent materials for which calculations are presented in this report are heavy concrete ($\rho$ = 3.5 g/cm$^3$), iron, lead, and uranium.

1.4 Pions

Calculations were made by assuming two different models for pion production: first, that due to Cocconi, Koester, and Perkins (CKP),[2] and second, that due to Trilling.[3] Current opinion indicates that the CKP formula seriously underestimates the number of high-energy pions. Recent calculations by Hagedorn and Ranft,[4] based upon a model of isobar production very similar to that of Trilling, give reasonably good agreement with Trilling's predictions for the pion spectra. Results for two choices of spectral functions are given here to enable one to gauge the magnitude of error in the shielding sizes (and costs) arising from the uncertainties in how to extrapolate the pion yield.

1.5 Energy

Results are presented for several primary energies which will be recognized as those of accelerators at present operating, under constructions, or being actively studied for the future.

1.6 Energy loss

For shields that are needed for biological protection we are

mainly concerned with the average behavior of muons, particularly with regard to their energy loss. (In certain neutrino experiments the fluctuations about the mean behavior have to be considered much more closely.) In addition to collision loss, contributions at high energy due to nuclear interaction, pair production, and bremsstrahlung are very significant,[5] and the calculated values of dE/dx used below are shown in Fig. 2. This figure clearly demonstrates the enhanced effectiveness of high-Z materials in degrading the energy of the muons.

## 2. General formulation

The number of protons interacting in the target (or effective target) per second is taken to be $N_0$. These give rise to pions of momentum p' at angle $\theta$ with respect to the forward direction. We write the double differential distribution of these pions as $d^2N/dp'd\Omega$ per proton-GeV/c-steradian. In drifting a distance $\Delta$ before striking the shield and interacting shortly thereafter, some of the pions decay to muons traveling in the same direction. The probability for such decay, assuming $\Delta$ to be much less than $\lambda p'$, is

$$\text{Decay probability} = \frac{\Delta}{\lambda p'}, \text{ where } \lambda = 55 \text{ m (GeV/c)}^{-1}. \qquad (1)$$

The decay of pions of momentum p' gives rise to a spectrum of muons with momentum p described by

$$\text{Muon spectrum} = \frac{dn}{dp} = \frac{1}{(1-k)p'} \text{ for } p' > p > kp' \qquad (2)$$

$$= 0 \text{ for } kp' > p > 0, \text{ where } k = 0.57.$$

Thus the momentum spectrum (per steradian, at angle $\theta$) of muons striking the shield is

$$\frac{d^2n}{dp\,d\Omega} = N_0 \int_p^{p_{max}} \frac{d^2N}{dp'\,d\Omega} \frac{\Delta}{\lambda p'} \frac{dp'}{(1-k)p'} \quad (GeV/c)^{-1}\ sr^{-1}\ sec^{-1}, \quad (3)$$

where $p_{max}$ equals either $p/k$ or $p_B$ (primary beam momentum), whichever is less. This is the maximum energy of a pion that can contribute by decay to a muon of momentum p.

We next consider the number of muons crossing an element of area dA at a position (r, L) in the shield (see Fig. 1). Since we consider only small values of $\theta$, $\cos\theta$ is taken to be unity and the element of area is perpendicular to the beam axis.

If we neglect the Coulomb scattering of the muons in the shield then the muons emerging through the element dA are those contained within a solid angle $d\Omega = dA/L^2$, produced at angle $\theta = r/L$ and having a range greater than $S = \frac{r-d}{\theta}$. Thus only muons above a minimum momentum p(S) contribute. We can write a suitable average momentum loss per meter as $\beta$, so that

$$p(S) = \beta S = \beta(r-d)/\theta = \beta L(1-d/r).$$

The flux of muons at the point (r, L) is then

$$\frac{dn}{dA} = \int_{p(S)}^{p_B} \frac{1}{L^2} \frac{d^2n}{dp\,d\Omega}\, dp$$

$$= \int_{p(S)}^{p_B} \frac{dp}{L^2} \int_p^{p_{max}} \frac{N_0\Delta}{\lambda(1-k)p'^2} \frac{d^2N}{dp'\,d\Omega}\, dp'\ m^{-2}\ sec^{-1}. \quad (4)$$

Setting $\frac{dn}{dA}$ equal to some desired design level, say M, leads to this equation for the profile of the shield in (r, L) coordinates, in the absence of Coulomb scattering. For the cavity or tunnel geometry $\Delta = d/\theta = Ld/r$. For the backstop geometry $\Delta$ is taken to be $1.8\ L_0$, where $L_0$ is the nuclear absorption mean free path (see below).

If we now include Coulomb scattering, we must consider that particles produced at angle $\theta$ undergo scattering and do not contribute to the flux through the element dA; likewise, particles produced at some other angle $\theta'$ suffer scattering that results in their emergence through the element dA under consideration. A new variable, $\phi$, now enters the problem, namely the angle between the plane containing the axis and the element dA and the plane containing the axis and the initial direction $\theta'$ of the particles ultimately scattered back through dA. In Fig. 1(b) the definition of $\phi$ is illustrated. The number of muons with momentum p that would (in the absence of Coulomb scattering) have passed through the element dA' at azimuthal angle $\phi$ and radial distance $r' = \theta'/L$ is (from Eq. 3)

$$\frac{d^2n}{dp\,dA'} = \frac{N_0}{L^2} \int_p^{p_{max}} \frac{d^2N'}{dp'\,d\Omega} \frac{\Delta'}{\lambda(1-k)p'^2}\, dp', \qquad (5)$$

where $$p \geq p(S') \text{ and } S' = \frac{r'-d}{\theta'} = L\left(1 - \frac{d}{r'}\right).$$

Here $\frac{d^2N'}{dp'\,d\Omega}$ is used to denote the value of the differential spectrum at angle $\theta' = r'/L$.

Because of Coulomb scattering some of these muons do not arrive in the element dA', but instead pass through dA. This contribution is given by

$$\frac{d^3n}{dA\,dA'dp} = \frac{d^2n}{dp\,dA'} \frac{1}{2\pi} \frac{1}{\sigma^2} \exp\left[-\frac{1}{2\sigma^2} |\underset{\sim}{r}-\underset{\sim}{r}'|^2\right], \tag{6}$$

where $\sigma$ is the standard deviation of the projected multiple scattering distribution for muons of initial momentum $p$ after they have passed through a thickness $S'$ of matter. Note that $\sigma$ depends on $p$ and $r'$ but not on $\phi$. The total number of muons of all momenta that scatter away from the direction of $dA'$ into the element $dA$ is obtained by integrating Eq. 6 over the momentum variable, viz.,

$$\frac{d^2n}{dA\,dA'} = \int_{p(S')}^{p_B} \frac{d^3n}{dA\,dA'dp}\, dp, \tag{7}$$

where $S' = (r'-d)/\theta' = L(1-d/r')$.

A further integration over the contributing elements of area, $dA' = r'\,dr'\,d\phi$, then yields the total contribution to the particles passing through $dA$. This assumes that the area $dA$ is surrounded by scattering material, whereas in fact $dA$ may be located on the surface of the shield. This is not too bad an assumption, because by far the greater contribution to the $r'$ integration comes from points with $r' < r$. Thus we have, finally,

$$\frac{dn}{dA} = \int_d^\infty r'\,dr' \int_0^{2\pi} \frac{d^2n}{dA\,dA'}\, d\phi$$

$$= \int_d^\infty r'\,dr' \int_0^{2\pi} d\phi \int_{p(S')}^{p_B} \left(\frac{d^3n}{dA\,dA'dp}\right) dp. \tag{8}$$

It is convenient to interchange the order of integration over p and $\phi$. After reordering and substituting from Eqs. 5 and 6, we have

$$\frac{dn}{dA} = C \int_d^\infty r' \Delta' \, dr' \int_{p(S')}^{p_B} \frac{1}{\sigma^2} e^{-(r^2+r'^2)/2\sigma^2} \, dp \int_0^{2\pi} e^{rr' \cos\theta/\sigma^2} \, d\phi$$

$$\times \int_p^{p_{max}} \frac{d^2N'}{dp' \, d\Omega} \frac{dp'}{p'^2} \text{ muons m}^{-2} \text{ sec}^{-1}, \qquad (9)$$

where $C = N_0/2\pi\lambda(1-k)L^2$.

Setting this equal to M (the constant desired level at the surface of the shield) defines the (r, L) equation of the shield profile.

3. Parameters and formulae used in the integrations

We now discuss the ingredients of the integral that have to be chosen in order to evaluate it. Several expressions have been proposed for the double differential source function for the pions.[2-4] Results are given later for the two cases

$$\text{CKP: } \frac{d^2N}{dp \, d\Omega} = \frac{n_\pi T}{2\pi p_0^2} \left(\frac{p}{T}\right)^2 e^{-p/T} e^{-p\theta/p_0}; \qquad (10a)$$

$$\text{Trilling: } \frac{d^2N}{dp \, d\Omega} = Ap^2 e^{-4.8p/\sqrt{p_B} - 2.6p\sqrt{p_B}\theta^2}$$

$$+ \frac{Bp^2}{p_B} e^{-10.4(p/p_B)^2} e^{-3.9p\theta}. \qquad (10b)$$

The Trilling formula[3] and also that proposed by Hagedorn and Ranft[4] predict many more high-energy pions from high-energy proton collisions than does the CKP formula.

The rms value, $\sigma$, of the Coulomb scattering distribution is given (see, for example, Ref. 1) by

$$\sigma^2 = \frac{(0.015)^2 \rho}{X_0} \int_0^S \frac{y^2\, dy}{(p_f + \beta y)^2} \quad \text{meter}^2, \tag{11}$$

where $p_f$ is the muon momentum after traversing the thickness S, and $\beta$ is the rate of momentum loss in GeV/c per meter. In general $\beta$ is a function of both y and $p_f$. If $\beta$ can be effectively treated as a constant, Eq. 11 can be written

$$\sigma^2 = \frac{(0.015)^2 \rho}{X_0} \frac{1}{\beta^3} p_i \left[ 1 - \left(\frac{p_f}{p_i}\right)^2 + 2\left(\frac{p_f}{p_i}\right) \ln \frac{p_f}{p_i} \right]. \tag{12}$$

This form gives adequate accuracy provided a suitable effective value of $\beta$ is chosen, viz. the average over the distance S through matter in which the muon momentum is reduced from $p_i$ to $p_f$. This is the form used in our computer program.

The values for the various constants used in evaluating Eqs. 10, 11, and 12 are given in Tables I and II.

Table I. Constants used in the flux formulae.

| | CKP | | | Trilling | | |
|---|---|---|---|---|---|---|
| $p_B$ (GeV/c) | $n_\pi$ | T | $p_0$ | $n_\pi$ | A | B |
| 25 | 1.01 | 3.36 | 0.22 | 1.32 | 3.30 | 4.16 |
| 70 | 1.33 | 7.68 | 0.22 | 1.84 | 3.30 | 4.16 |
| 200 | 1.69 | 16.20 | 0.22 | 2.91 | 3.30 | 4.16 |
| 300 | 1.87 | 21.75 | 0.22 | 3.55 | 3.30 | 4.16 |

Table II. Constants used for different materials.

| Material | $\rho$ (g/m$^3$) ($\times 10^6$) | $L_0$ (gm/m$^2$) ($\times 10^4$) | $X_0$ (g/m$^2$) ($\times 10^4$) |
|---|---|---|---|
| Heavy concrete | 3.49 | 134 | 12.85 |
| Iron | 7.8 | 134 | 13.8 |
| Lead | 11.34 | 202 | 5.8 |
| Uranium | 18.7 | 210 | 5.5 |

The value to be inserted for $\Delta$ in Eq. 9 depends upon the geometry of the situation. The following expressions were used in the calculations:

(1) Cylindrical cavity or tunnel: $\Delta = d/\theta$,

where d = radius of cavity or tunnel,

$\theta$ = angle of production of the pions;

(2) Backstop: $\Delta = 1.8\ L_0$,

where $L_0$ = nuclear absorption mean free path in the backstop material (see Table II).

Thus for the cylindrical cavity we assume that the pions are absorbed the moment they strike the material of the shield, and that only the distance between the target and the point of impact need be considered for occurrence of the $\pi \rightarrow \mu$ decay. Because we further assume that major interest in the shield thickness is near the forward direction, the approximation $\sin\theta \approx \theta$ is made. Thus the flux calculation should be useful out to angles $\theta \approx 30$ to 40 deg, which is far beyond the point where the production formulae, Eqs. 10a and 10b, are valid.

In the backstop geometry it is not obvious that $\Delta$ can be taken as a constant (for a given material). The justification for this is based

upon the cascade calculations by Riddell.[6] He used the Trilling formulae (Eq. 10b) for the production of pions by nucleons, and other calculations by Trilling[5] for the production of nucleons by nucleons, and calculated the flux of pions and nucleons at various depths in homogeneous absorbers of different atomic weight. By integrating over pion energy and the probability of decay to a muon, and finally integrating over the thickness of the absorber, one can derive a differential momentum spectrum for the muons that are produced. The results of such a calculation for copper ($L_0$ = 18 cm) are shown by the solid curve in Fig. 3. Also shown for comparison (dashed curve) is the flux of muons produced when pions emerge from a point target and are allowed to decay for 1 meter downstream from the target, viz.,

$$\frac{dn_\mu}{dp} = \int \frac{d^2n}{dp\, d\Omega}\, d\Omega\,, \qquad (13)$$

where the integrand is given by Eq. 3 with $\Delta$ = 1 meter, and $\frac{d^2N}{dp\, d\Omega}$ is taken from Eq. 10b. Both curves are very similar in shape, but displaced from each other by a factor of three. We therefore have assumed that Eq. 3 is a valid description of the muon flux, provided a suitable constant effective value for $\Delta$ is inserted. For copper, $\Delta$ = 33 cm = 1.8 $L_0$, and because the decay probability scales linearly with absorption mean free path in this model, the value $\Delta = 1.8\ L_0$ is used for other materials. All the muons are assumed to be born at the point of impact of the protons with the shield rather than distributed over the first few mean free paths. This is justified because the length 1.8 $L_0$ is negligible compared with the typical dimensions of the shield at small angles ($\sin\theta \approx \theta$).

4. Results

A computer program was written for the Lawrence Radiation Laboratory CDC 6600 to evaluate the muon flux $\frac{dn}{dA}$ in units of muons $(\text{meter})^{-2}$ $(\text{incident proton})^{-1}$ $(\text{sec})^{-1}$, as given by Eq. 9 with $N_0 = 1$. A particular value of L was inserted and the flux calculated at a shield radius r; thereafter an iterative process was used whereby r was varied until dn/dA equaled the desired value M. Since $N_0$ will be in the region of $10^{13}$ protons $\text{sec}^{-1}$, and the tolerance value for fast muons is of the order of $10^5$ muons $\text{meter}^{-2}$ $\text{second}^{-1}$, the (r, L) equation of the shield profile was printed out for values of $M = 10^{-9}$, $10^{-8}$, $10^{-7}$, $10^{-6}$.

In evaluating Eq. 9 the leftmost integral over r' should in principle be taken from r' = d to r' = ∞, where d = 0 for the backstop case. In fact, this integral was evaluated numerically by a trapezoidal rule from r' = d to r' = R, where R was taken to be 20 cm greater than r, the radius of the shield. The contribution to the integral from values of r' > r is small and the value 20 cm is not critical. The azimuthal integral in Eq. 9 can be written

$$\int_0^{2\pi} e^{rr' \cos\theta/\sigma^2} \, d\phi = 2\pi I_0 \left(\frac{rr'}{\sigma^2}\right),$$

where $I_0(z)$ is the usual symbol for the modified Bessel function. This was evaluated by a standard library subroutine.

It is of interest in understanding the behavior of the muons in the shield to isolate separately the effects of Coulomb-scattering diffusion and of production-angular divergence. Arrangements were made in

the program whereby the effect of Coulomb scattering was made negligible and the profile of the shield calculated, assuming all lateral angular spread was due to the initial angular spread of the pions. On the other hand, the profile could also be calculated on the assumption that all production angles were zero and the only lateral diffusion was due to scattering. Examples of such calculations for backstops of four materials and for $M = 10^{-8}$ are shown in Fig. 4, where the CKP pion-production spectrum was used. It is clear from these curves that the relative importance of the two effects varies throughout the shield length, but that they both remain comparable to each other. Near the front of the shield the lateral dimension is determined mainly by production angle. The scattering effects help in allowing a shorter overall length of the shield. The remaining graphs (Figs. 5 through 38) show shield profiles calculated from Eq. 9 by using the CKP and Trilling production distributions at four flux levels ($M = 10^{-6}$, $10^{-7}$, $10^{-8}$, $10^{-9}$). They are organized as follows:

| Figure numbers | Incident proton momentum (BeV/c) |
|---|---|
| 5 through 11 | 25 |
| 12 through 20 | 70 |
| 21 through 29 | 200 |
| 30 through 38 | 300 |

The profiles refer to calculations for a backstop and a long cylindrical cavity of inner radius d = 0.15 cm. The latter is a geometry appropriate to the transport of an extracted proton beam down a pipe

with close-packed shielding around it. In addition, results are shown for d = 2.0 m for barytes concrete only, which is a geometry appropriate to the shielding of a proton beam in a fairly large tunnel.

## References

1. D. Keefe, Mu-Meson Shielding: Approximate Calculations, Lawrence Radiation Laboratory Report UCID-10018, 1964 (unpublished).
2. G. Cocconi, L. J. Koester, and D. H. Perkins, Berkeley High Energy Physics Study, Lawrence Radiation Laboratory Report UCRL-10022, 1962, p. 167 (unpublished).
3. G. H. Trilling, Pion and Proton Fluxes from High Energy Proton Collisions, Lawrence Radiation Laboratory Report UCRL-16830, 1966, p. 25 (unpublished).
4. R. Hagedorn and J. Ranft, Momentum Spectra of Particles Produced in High-Energy pp Collisions, CERN/ECFA 67/16, Vol. 1, 1967, p. 69 (unpublished).
5. See for example: R. H. Thomas, Energy Loss of High-Energy Muons, Lawrence Radiation Laboratory Report UCID-10010, 1964 (unpublished).
6. R. J. Riddell, Jr., High-Energy Nuclear Cascades in Matter, Lawrence Radiation Laboratory Report UCRL-11989, 1965 (unpublished).

## List of figures

| | | | |
|---|---|---|---|
| 20. | Flux contours: | 70 GeV, Tunnel: | heavy concrete. |
| 21. | Flux contours: | 200 GeV, Backstop: | heavy concrete. |
| 22. | Flux contours: | 200 GeV, Backstop: | iron. |
| 23. | Flux contours: | 200 GeV, Backstop: | lead. |
| 24. | Flux contours: | 200 GeV, Backstop: | uranium. |
| 25. | Flux contours: | 200 GeV, Cavity: | heavy concrete. |
| 26. | Flux contours: | 200 GeV, Cavity: | iron. |
| 27. | Flux contours: | 200 GeV, Cavity: | lead. |
| 28. | Flux contours: | 200 GeV, Cavity: | uranium. |
| 29. | Flux contours: | 200 GeV, Tunnel: | heavy concrete. |
| 30. | Flux contours: | 300 GeV, Backstop: | heavy concrete. |
| 31. | Flux contours: | 300 GeV, Backstop: | iron. |
| 32. | Flux contours: | 300 GeV, Backstop: | lead. |
| 33. | Flux contours: | 300 GeV, Backstop: | uranium. |
| 34. | Flux contours: | 300 GeV, Cavity: | heavy concrete. |
| 35. | Flux contours: | 300 GeV, Cavity: | iron. |
| 36. | Flux contours: | 300 GeV, Cavity: | lead. |
| 37. | Flux contours: | 300 GeV, Cavity: | uranium. |
| 38. | Flux contours: | 300 GeV, Tunnel: | heavy concrete. |

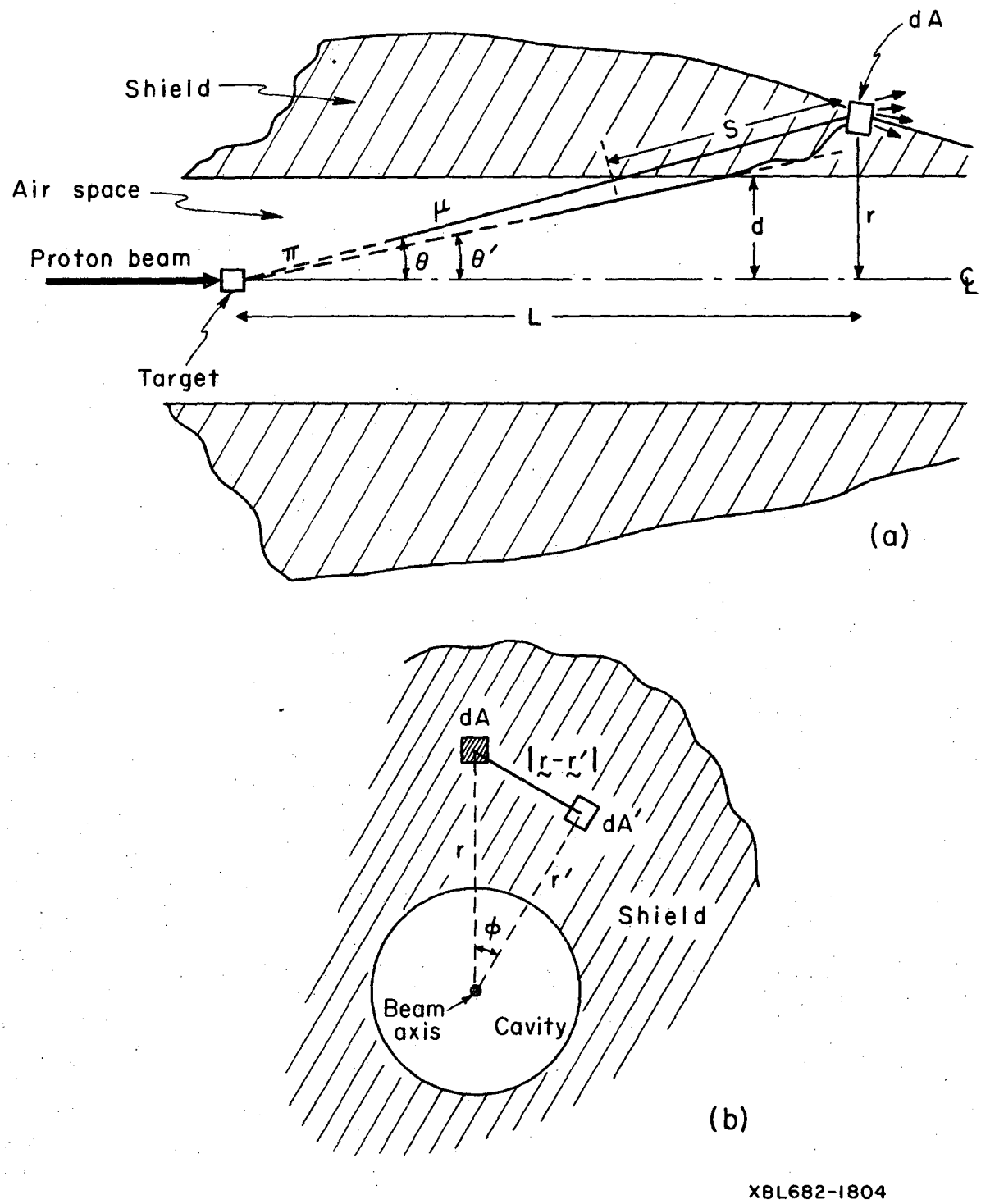
dA
Shield
S
Air space
μ
d
r
Proton beam
π
θ
θ′
L
Target
(a)
dA
|r-r′|
dA′
r
r′
Shield
ϕ
Beam axis
Cavity
(b)
XBL682-1804

Fig. 1

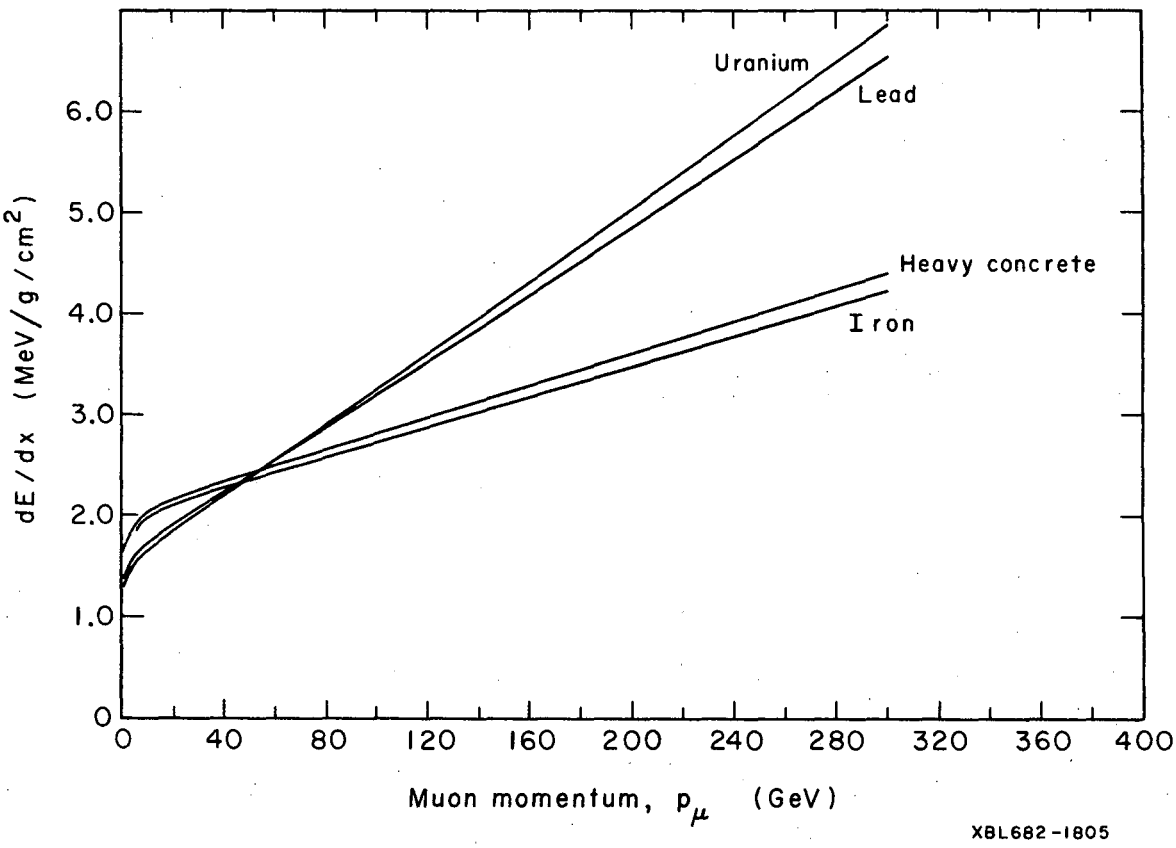
Uranium
Lead
Heavy concrete
Iron
dE/dx (MeV/g/cm²)
0
1.0
2.0
3.0
4.0
5.0
6.0
0
40
80
120
160
200
240
280
320
360
400
Muon momentum, $p_\mu$ (GeV)
XBL682-1805

Fig. 2

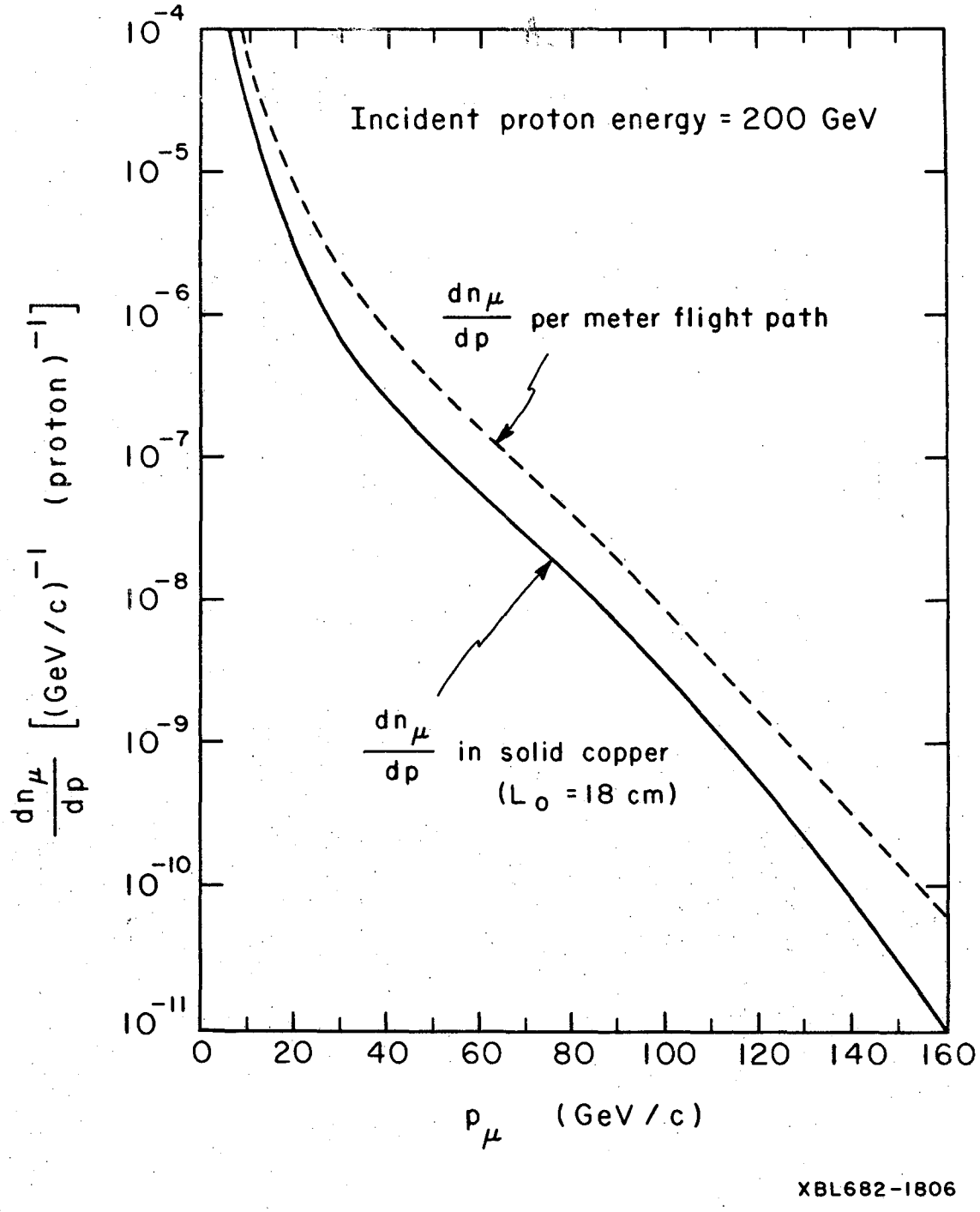
Incident proton energy = 200 GeV
$\frac{dn_\mu}{dp}$ per meter flight path
$\frac{dn_\mu}{dp}$ in solid copper
($L_0$ = 18 cm)
$\frac{dn_\mu}{dp}$ [(GeV/c)$^{-1}$ (proton)$^{-1}$]
$p_\mu$ (GeV/c)
$10^{-4}$
$10^{-5}$
$10^{-6}$
$10^{-7}$
$10^{-8}$
$10^{-9}$
$10^{-10}$
$10^{-11}$
0 20 40 60 80 100 120 140 160
XBL682-1806

Fig. 3

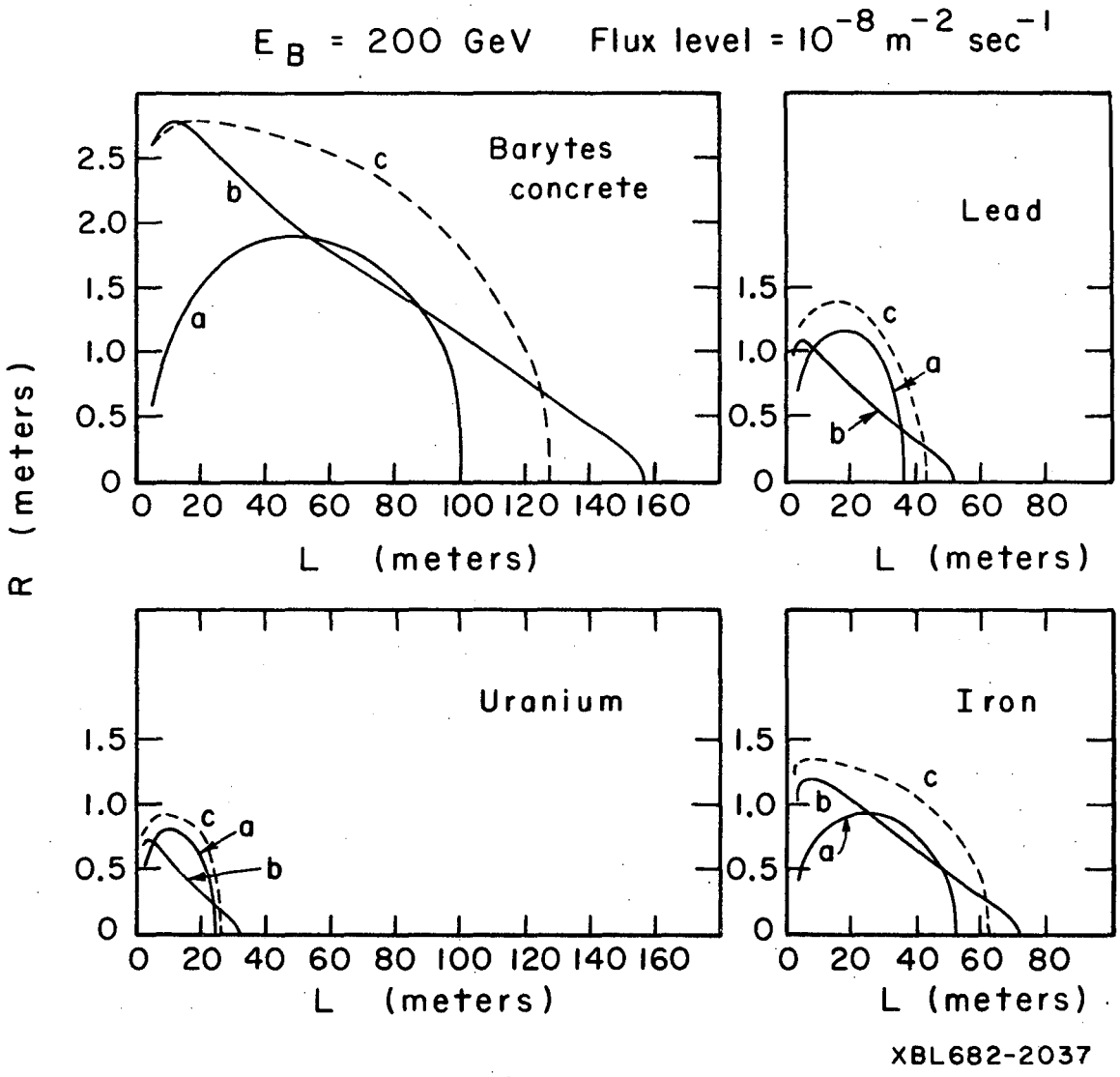
$E_B$ = 200 GeV Flux level = $10^{-8}$ $m^{-2}$ $sec^{-1}$
Barytes concrete
Lead
Uranium
Iron
R (meters)
L (meters)
a
b
c
0 20 40 60 80 100 120 140 160
0 20 40 60 80
0 0.5 1.0 1.5 2.0 2.5
XBL682-2037

Fig. 4

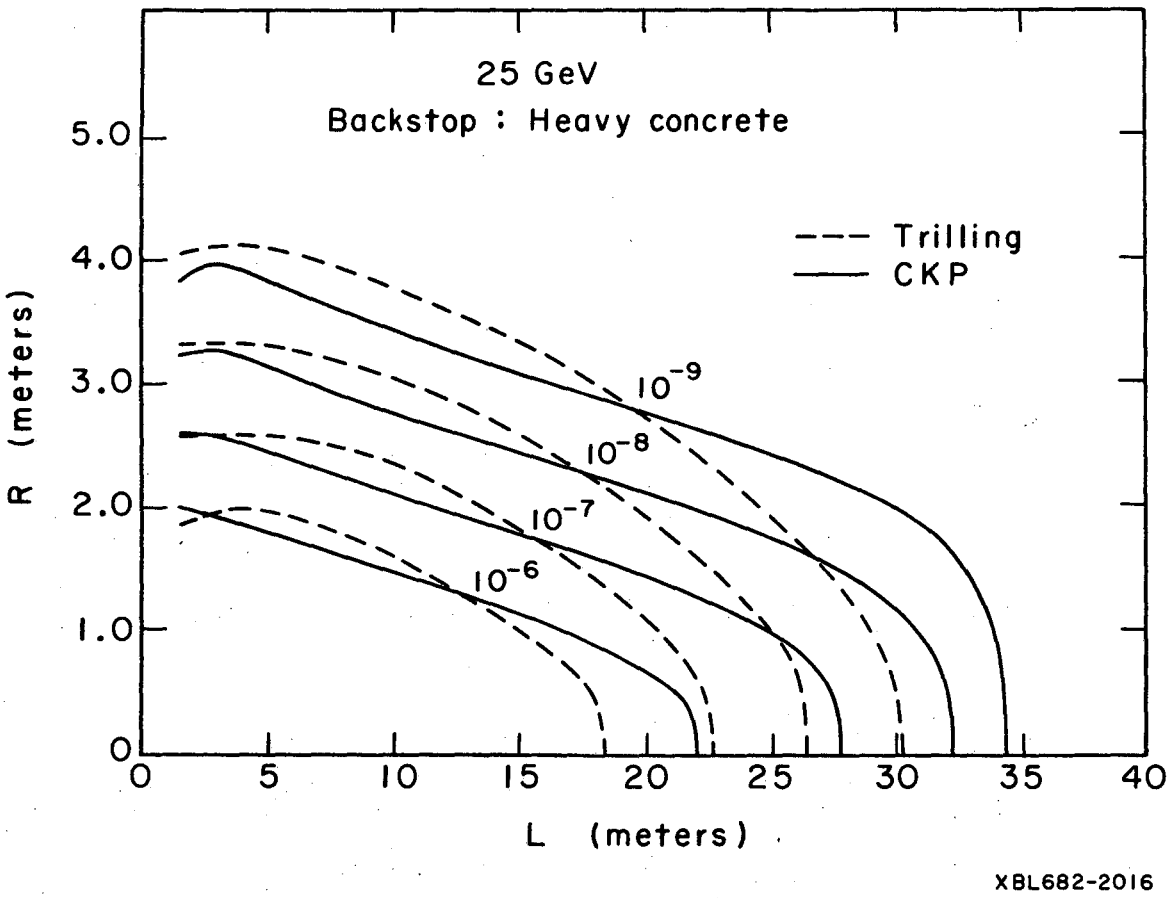
25 GeV
Backstop : Heavy concrete
Trilling
CKP
$10^{-9}$
$10^{-8}$
$10^{-7}$
$10^{-6}$
R (meters)
L (meters)
0
1.0
2.0
3.0
4.0
5.0
0
5
10
15
20
25
30
35
40
XBL682-2016

Fig. 5

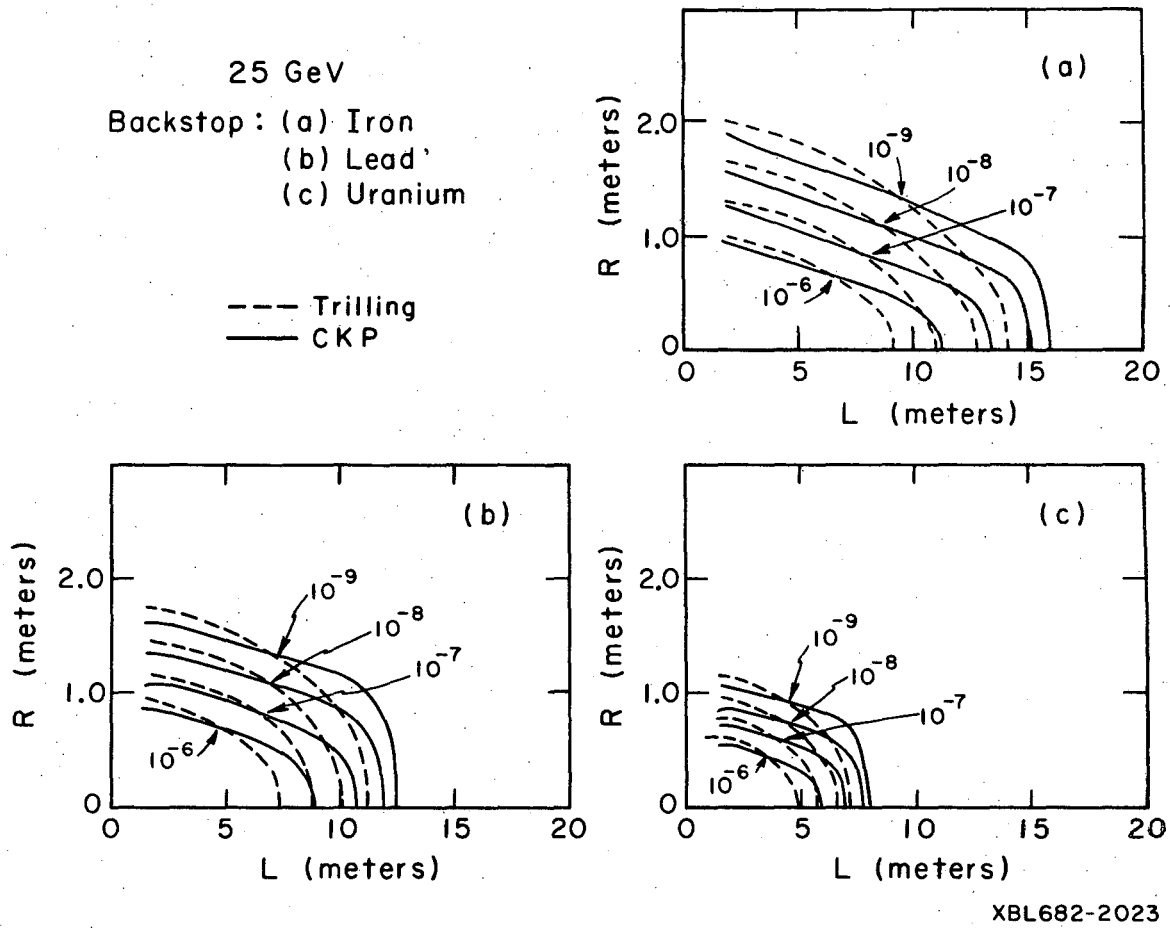
25 GeV
Backstop : (a) Iron
(b) Lead
(c) Uranium
--- Trilling
—— CKP
(a)
(b)
(c)
R (meters)
L (meters)
$10^{-9}$
$10^{-8}$
$10^{-7}$
$10^{-6}$
0
1.0
2.0
5
10
15
20
XBL682-2023

Fig. 6

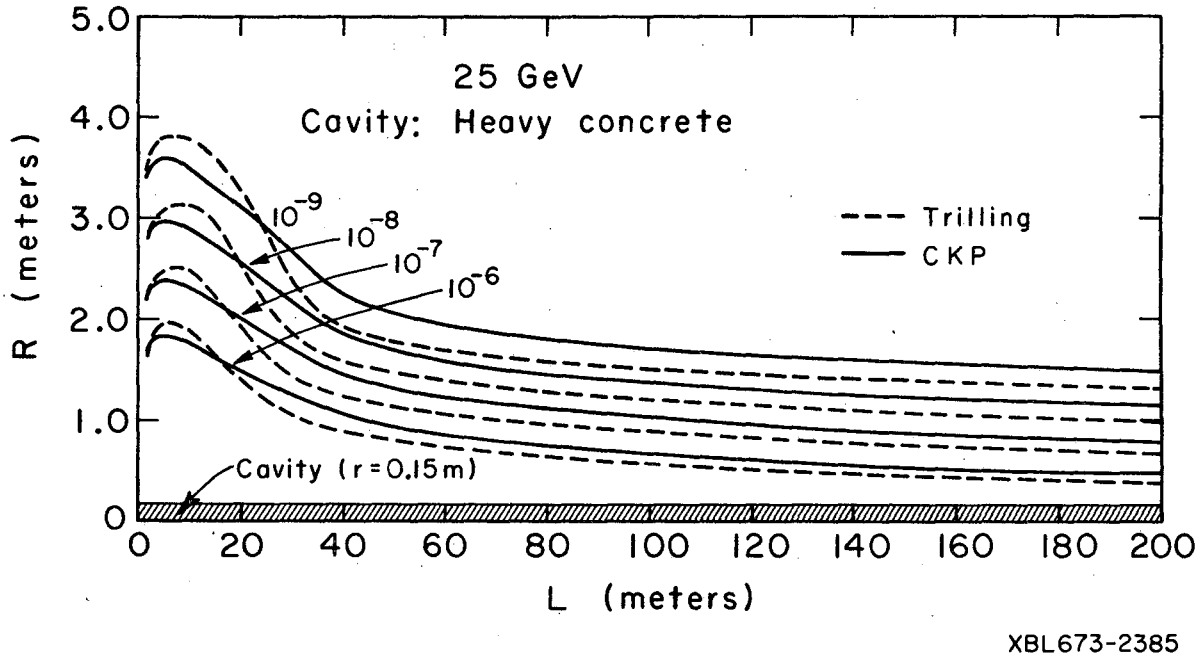
25 GeV
Cavity: Heavy concrete
Trilling
CKP
$10^{-9}$
$10^{-8}$
$10^{-7}$
$10^{-6}$
Cavity (r=0.15m)
R (meters)
L (meters)
0
1.0
2.0
3.0
4.0
5.0
0
20
40
60
80
100
120
140
160
180
200
XBL673-2385

Fig. 7

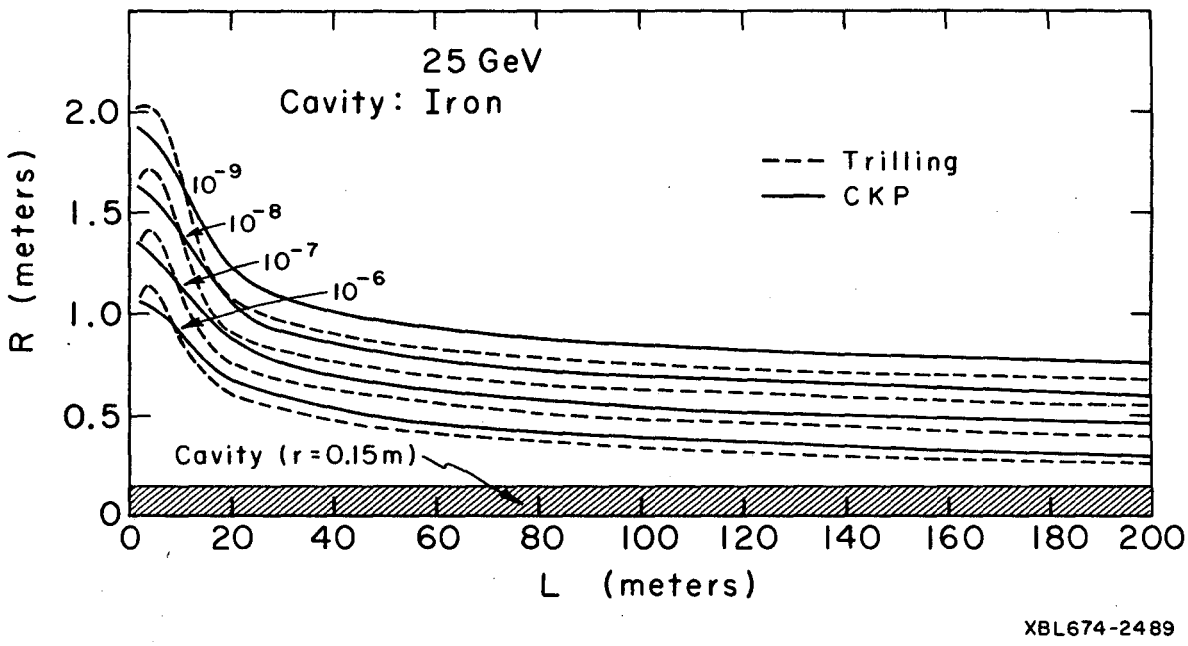
25 GeV
Cavity: Iron
--- Trilling
—— CKP
$10^{-9}$
$10^{-8}$
$10^{-7}$
$10^{-6}$
Cavity (r=0.15m)
R (meters)
L (meters)
0
0.5
1.0
1.5
2.0
0
20
40
60
80
100
120
140
160
180
200
XBL674-2489

Fig. 8

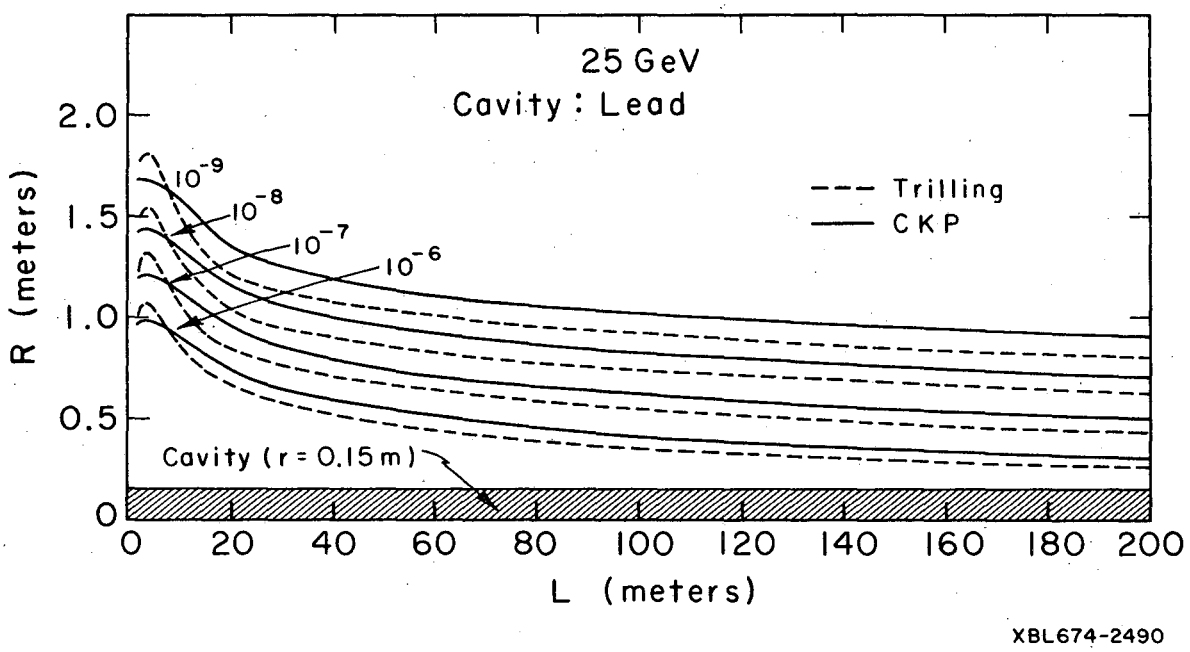
25 GeV
Cavity : Lead
Trilling
CKP
$10^{-9}$
$10^{-8}$
$10^{-7}$
$10^{-6}$
Cavity (r = 0.15 m)
R (meters)
L (meters)
0
0.5
1.0
1.5
2.0
0
20
40
60
80
100
120
140
160
180
200
XBL674-2490

Fig. 9

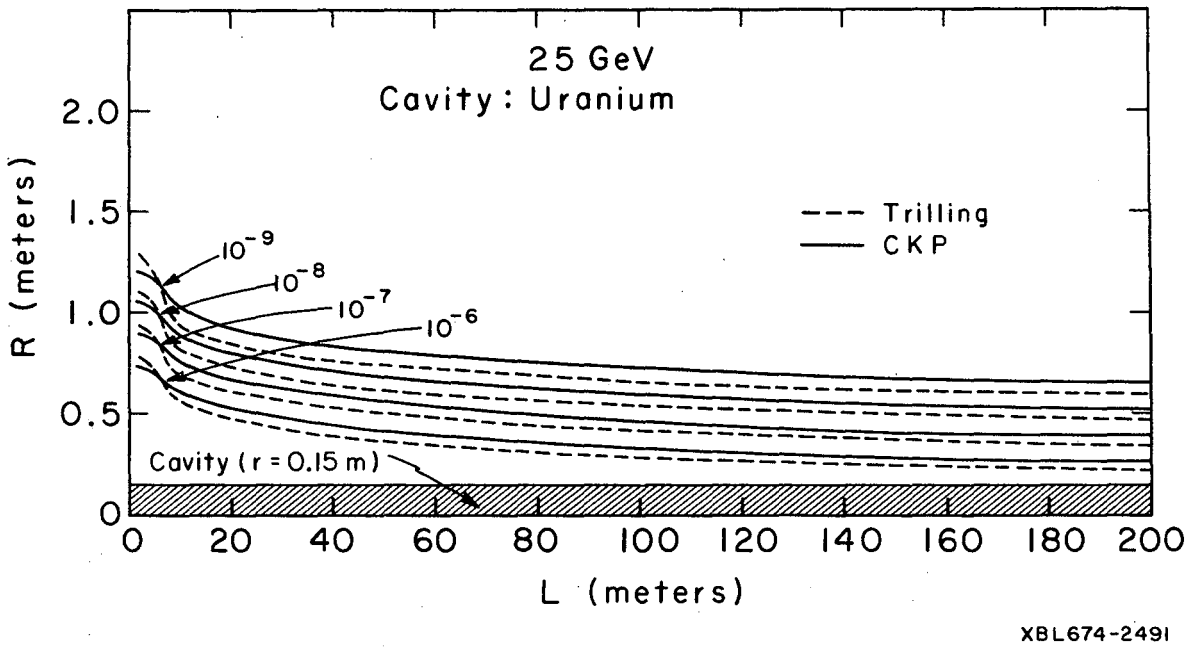
25 GeV
Cavity : Uranium
Trilling
CKP
$10^{-9}$
$10^{-8}$
$10^{-7}$
$10^{-6}$
Cavity (r = 0.15 m)
R (meters)
L (meters)
0
0.5
1.0
1.5
2.0
0
20
40
60
80
100
120
140
160
180
200
XBL674-2491

Fig. 10

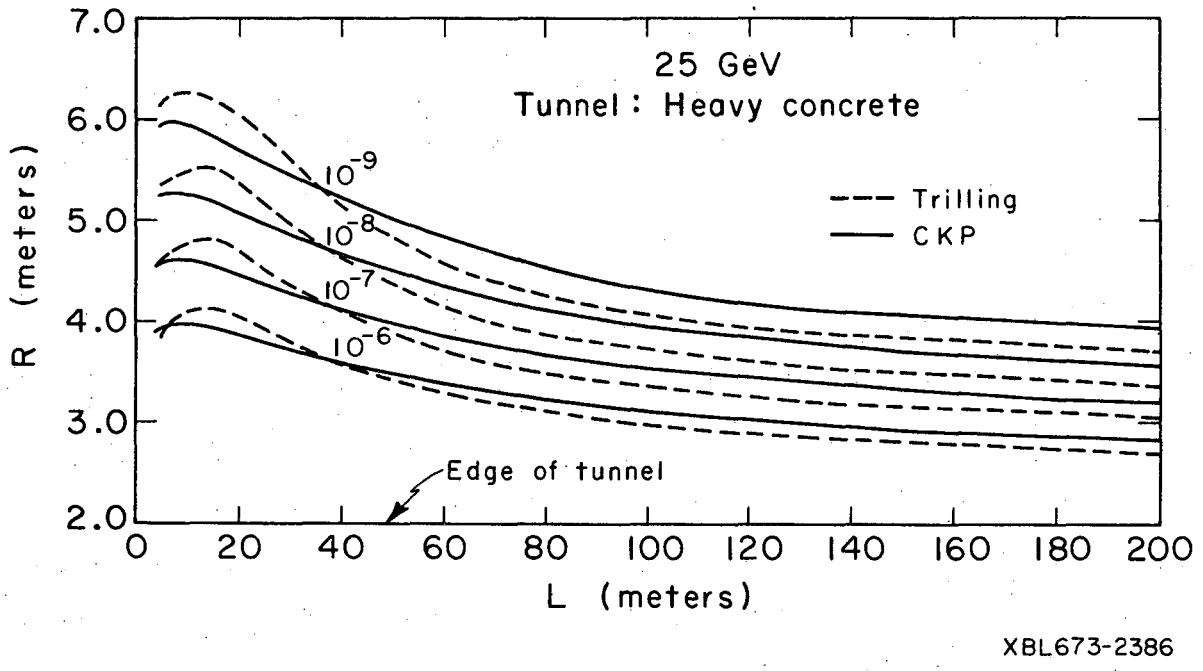
25 GeV
Tunnel : Heavy concrete
Trilling
CKP
$10^{-9}$
$10^{-8}$
$10^{-7}$
$10^{-6}$
Edge of tunnel
R (meters)
L (meters)
7.0
6.0
5.0
4.0
3.0
2.0
0
20
40
60
80
100
120
140
160
180
200
XBL673-2386

Fig. 11

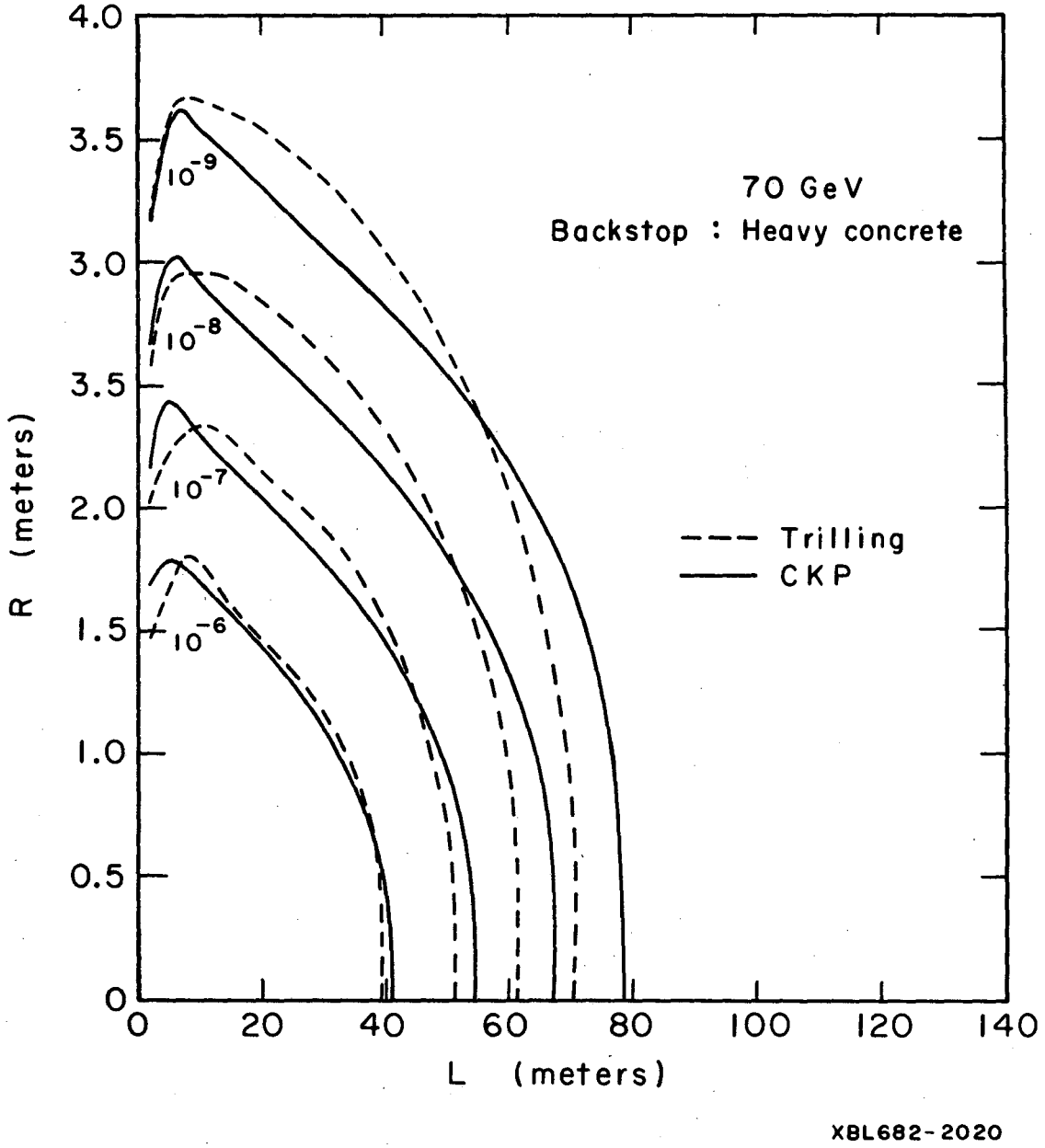
4.0
3.5
3.0
3.5
2.0
1.5
1.0
0.5
0
R (meters)
$10^{-9}$
$10^{-8}$
$10^{-7}$
$10^{-6}$
70 GeV
Backstop : Heavy concrete
Trilling
CKP
0
20
40
60
80
100
120
140
L (meters)
XBL682-2020

Fig. 12

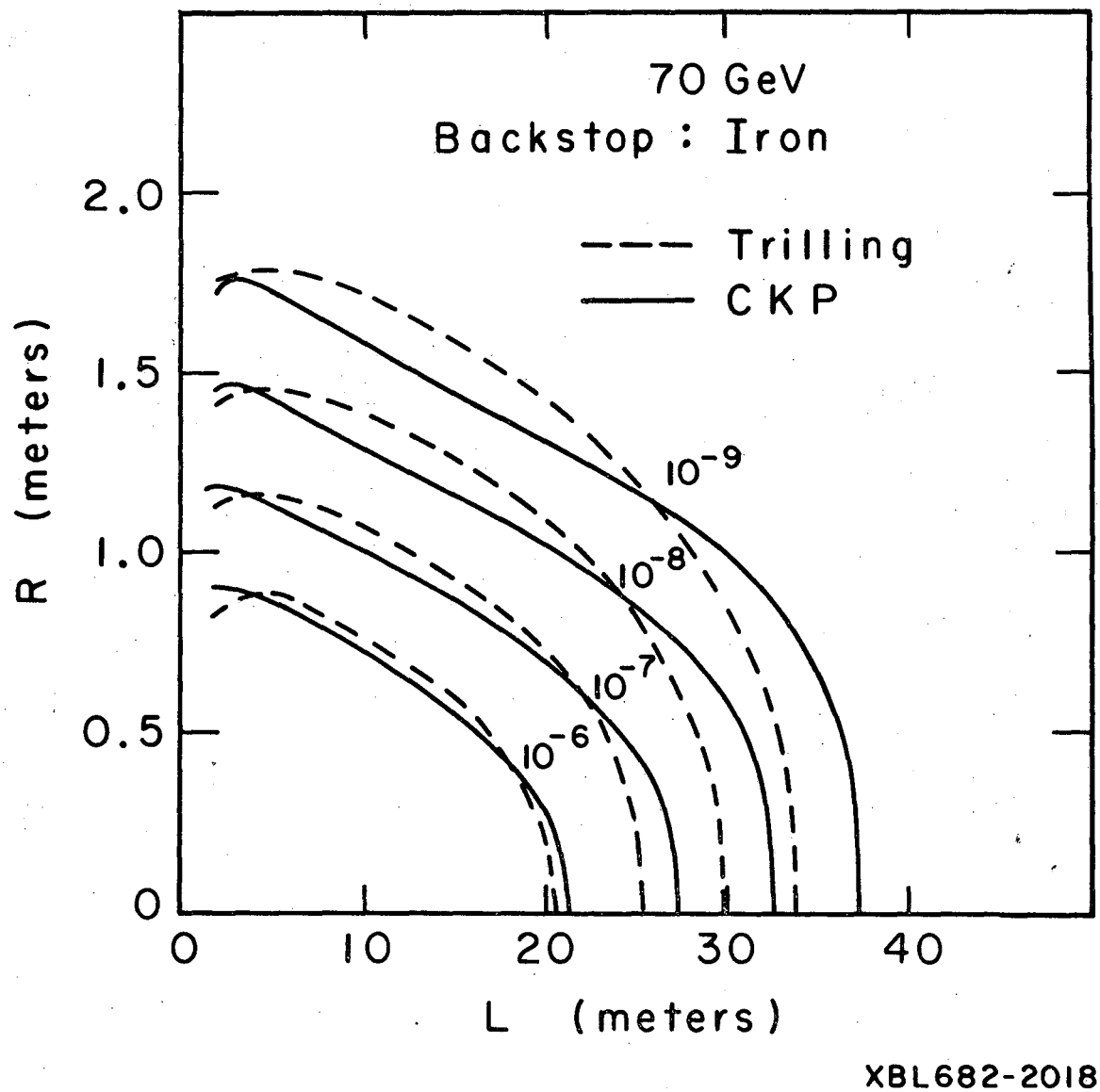
70 GeV
Backstop : Iron
Trilling
CKP
$10^{-9}$
$10^{-8}$
$10^{-7}$
$10^{-6}$
R (meters)
L (meters)
0
0.5
1.0
1.5
2.0
0
10
20
30
40
XBL682-2018

Fig. 13

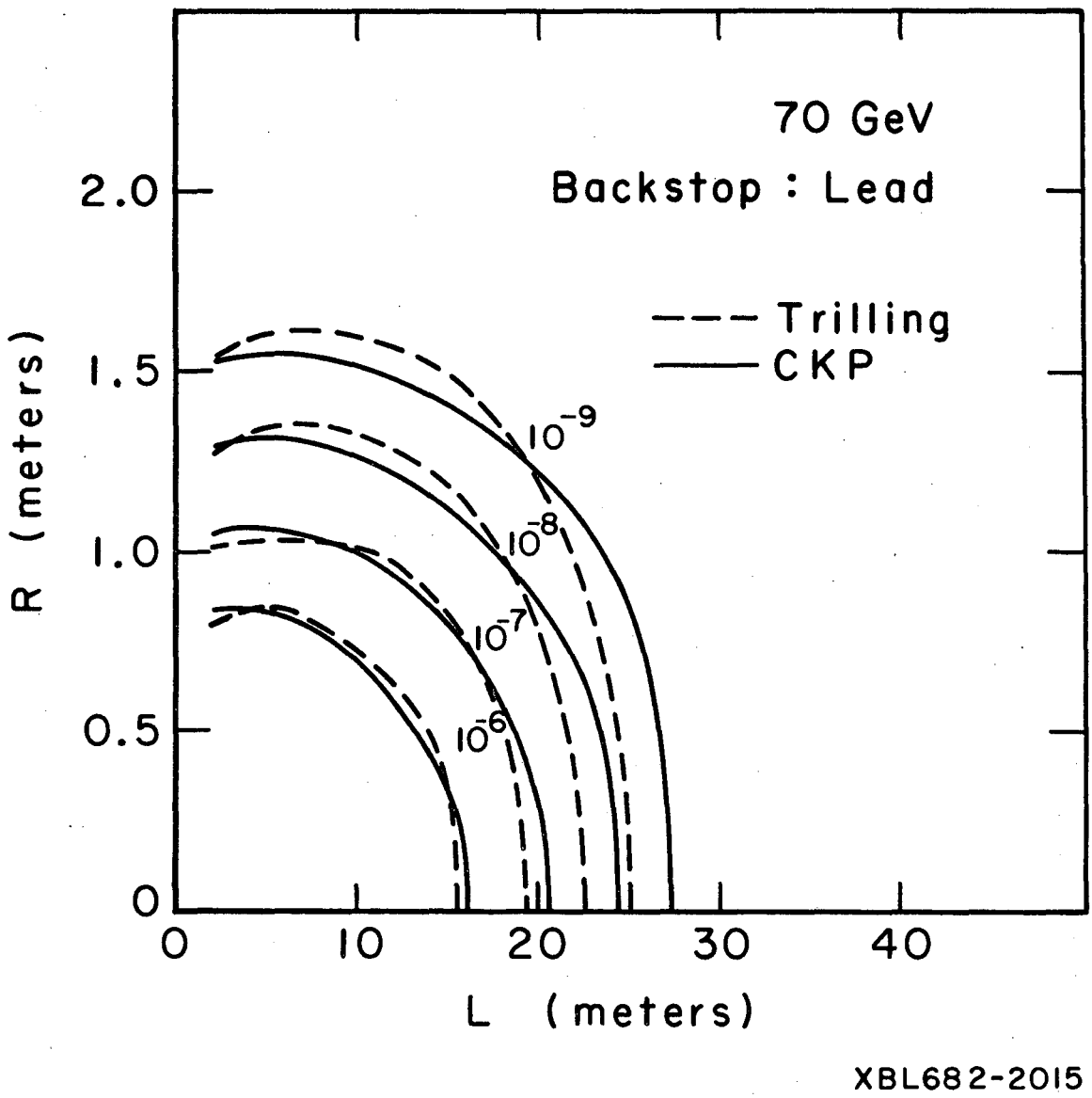
70 GeV
Backstop : Lead
Trilling
CKP
$10^{-9}$
$10^{-8}$
$10^{-7}$
$10^{-6}$
R (meters)
L (meters)
0
0.5
1.0
1.5
2.0
0
10
20
30
40
XBL682-2015

Fig. 14

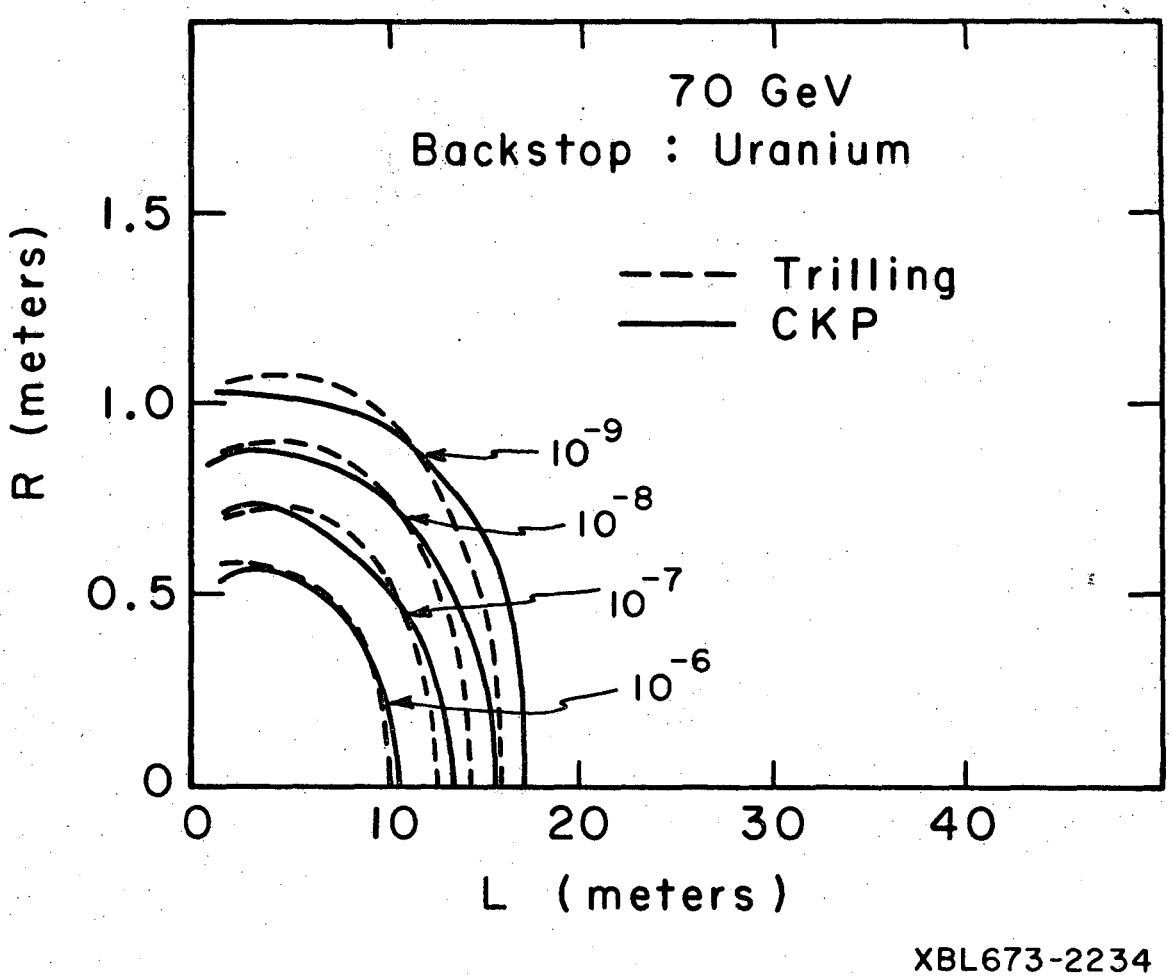
70 GeV
Backstop : Uranium
Trilling
CKP
$10^{-9}$
$10^{-8}$
$10^{-7}$
$10^{-6}$
R (meters)
L (meters)
0
0.5
1.0
1.5
0
10
20
30
40
XBL673-2234

Fig. 15

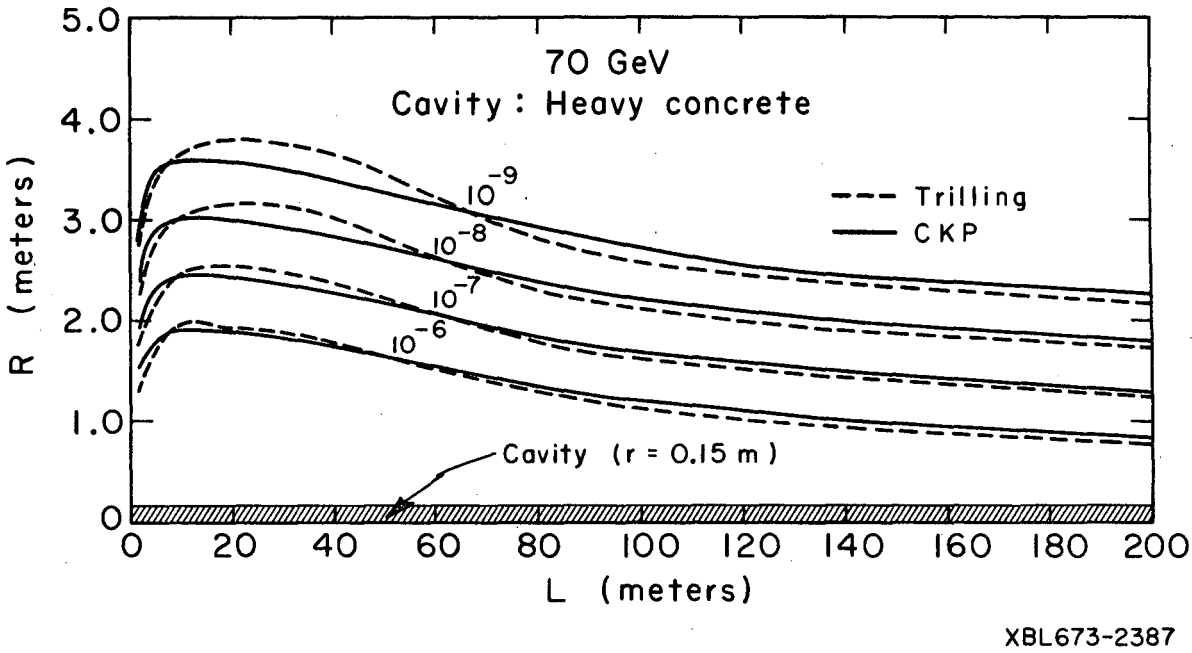
70 GeV
Cavity : Heavy concrete
Trilling
CKP
$10^{-9}$
$10^{-8}$
$10^{-7}$
$10^{-6}$
Cavity (r = 0.15 m)
R (meters)
L (meters)
0
1.0
2.0
3.0
4.0
5.0
0
20
40
60
80
100
120
140
160
180
200
XBL673-2387

Fig. 16

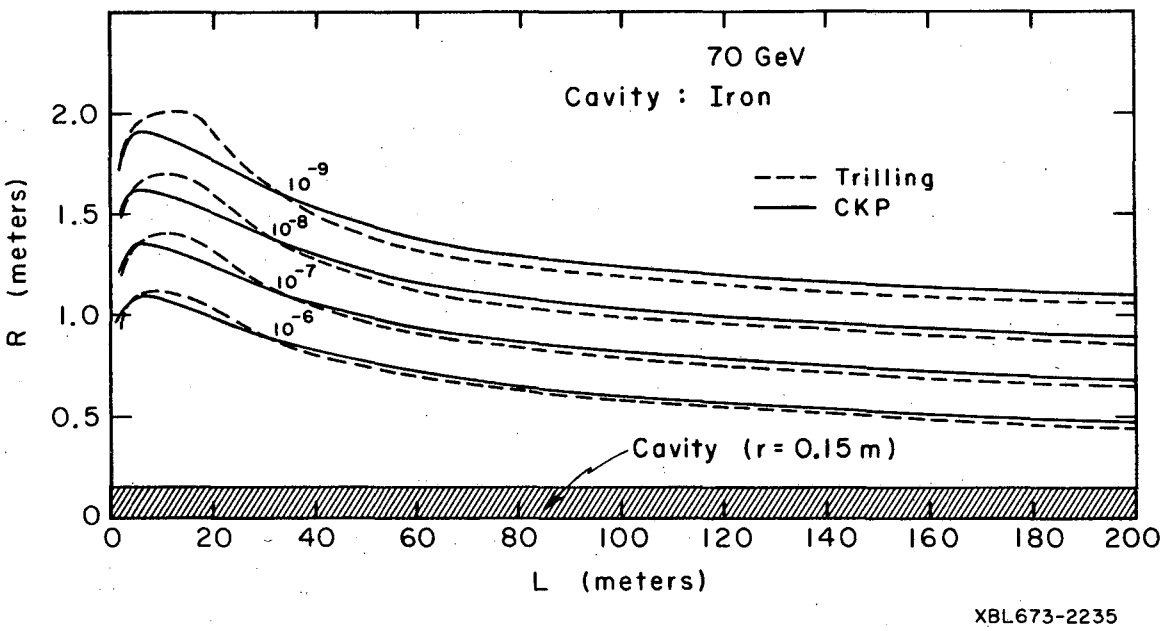
70 GeV
Cavity : Iron
Trilling
CKP
$10^{-9}$
$10^{-8}$
$10^{-7}$
$10^{-6}$
Cavity (r = 0.15 m)
R (meters)
L (meters)
0
0.5
1.0
1.5
2.0
0
20
40
60
80
100
120
140
160
180
200
XBL673-2235

Fig. 17

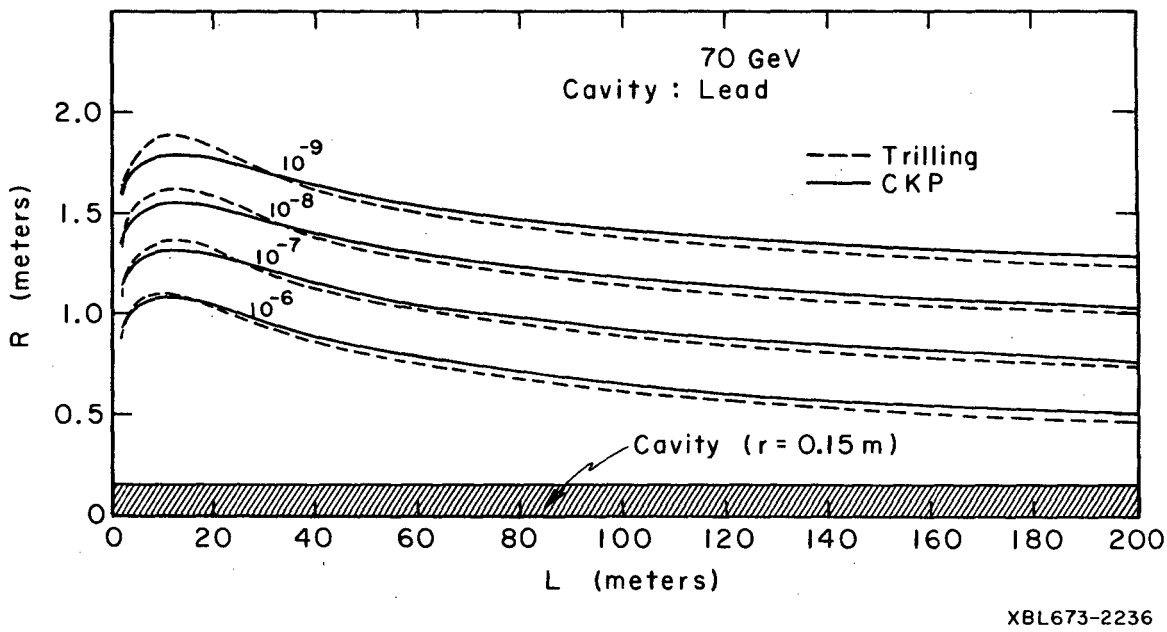
70 GeV
Cavity : Lead
Trilling
CKP
$10^{-9}$
$10^{-8}$
$10^{-7}$
$10^{-6}$
Cavity (r = 0.15 m)
R (meters)
L (meters)
0
0.5
1.0
1.5
2.0
0
20
40
60
80
100
120
140
160
180
200
XBL673-2236

Fig. 18

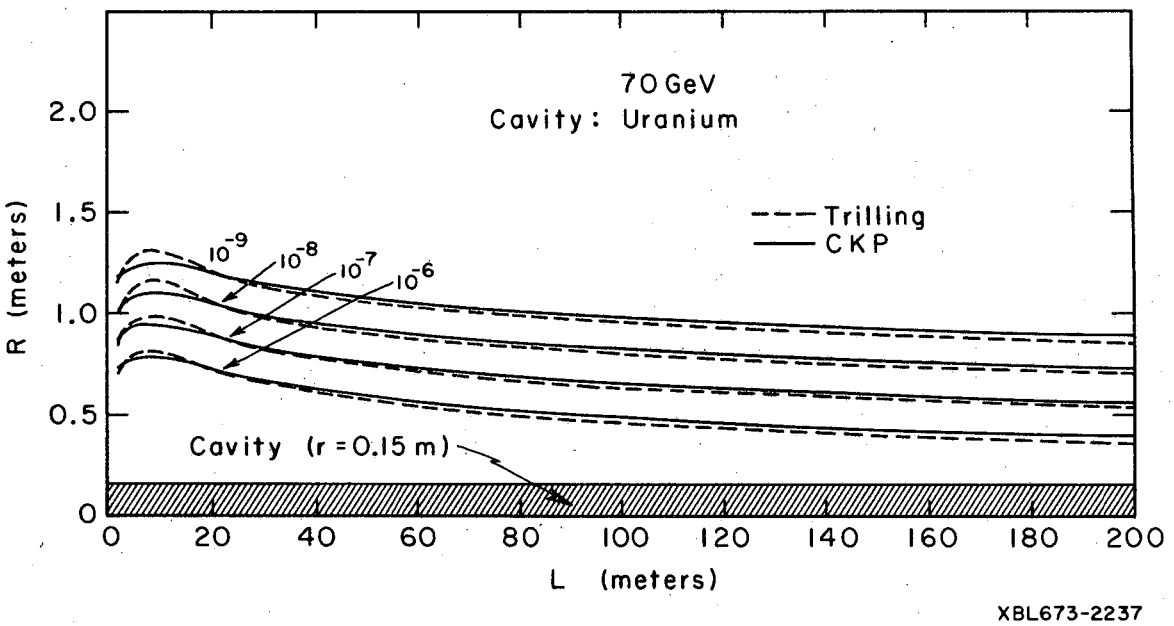
70 GeV
Cavity: Uranium
Trilling
CKP
$10^{-9}$
$10^{-8}$
$10^{-7}$
$10^{-6}$
Cavity (r = 0.15 m)
R (meters)
L (meters)
0
0.5
1.0
1.5
2.0
0
20
40
60
80
100
120
140
160
180
200
XBL673-2237

Fig. 19

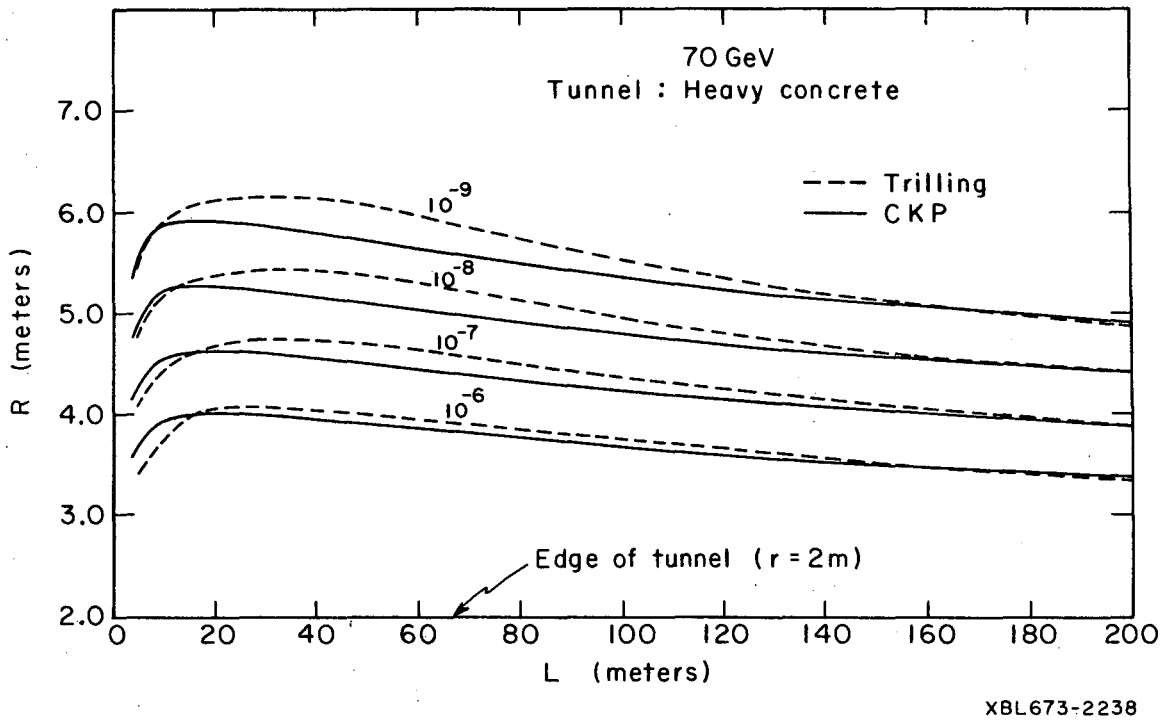
70 GeV
Tunnel : Heavy concrete
Trilling
CKP
$10^{-9}$
$10^{-8}$
$10^{-7}$
$10^{-6}$
Edge of tunnel (r = 2m)
R (meters)
L (meters)
7.0
6.0
5.0
4.0
3.0
2.0
0
20
40
60
80
100
120
140
160
180
200
XBL673-2238

Fig. 20

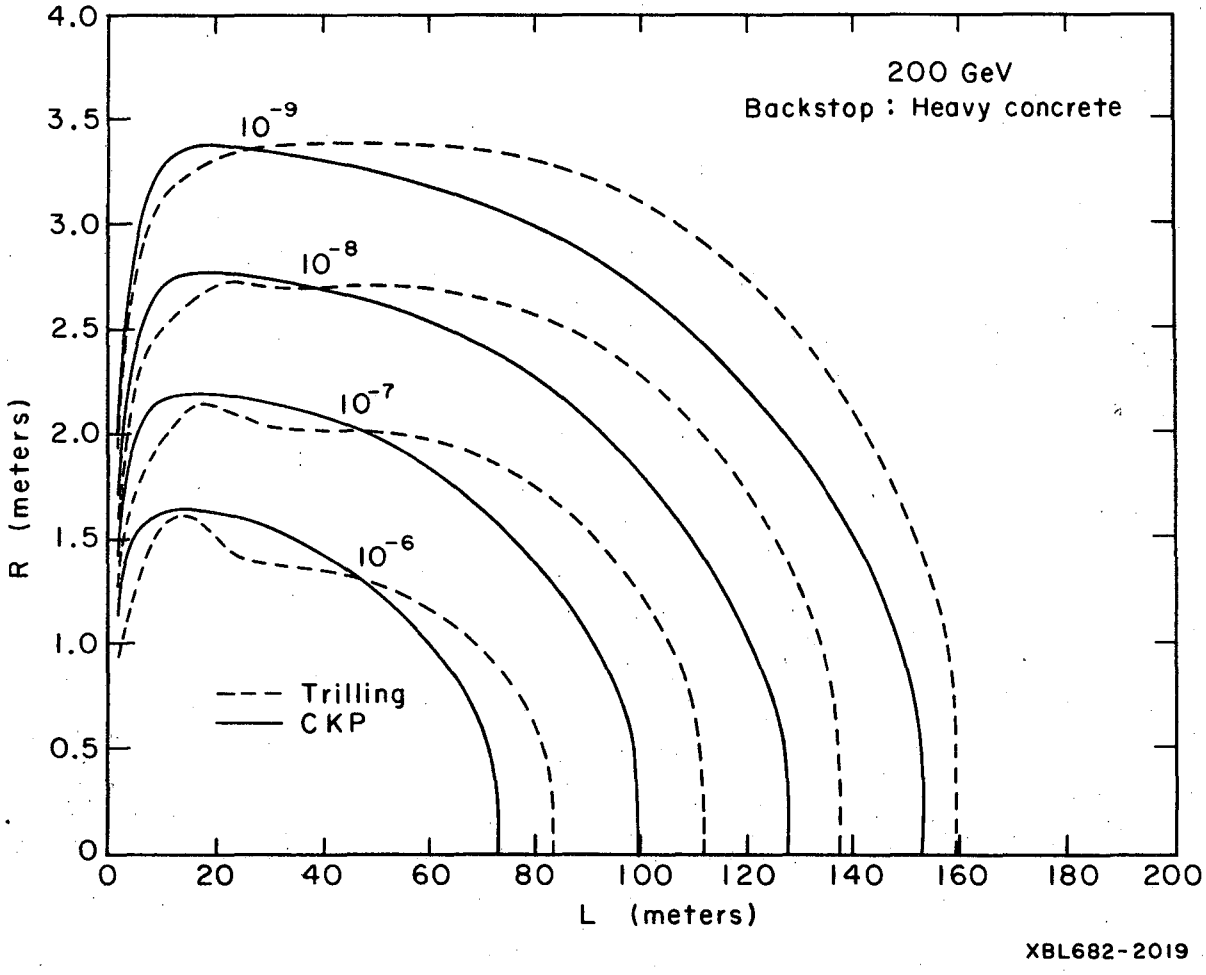
200 GeV
Backstop : Heavy concrete
$10^{-9}$
$10^{-8}$
$10^{-7}$
$10^{-6}$
Trilling
CKP
R (meters)
L (meters)
0
0.5
1.0
1.5
2.0
2.5
3.0
3.5
4.0
0
20
40
60
80
100
120
140
160
180
200
XBL682-2019

Fig. 21

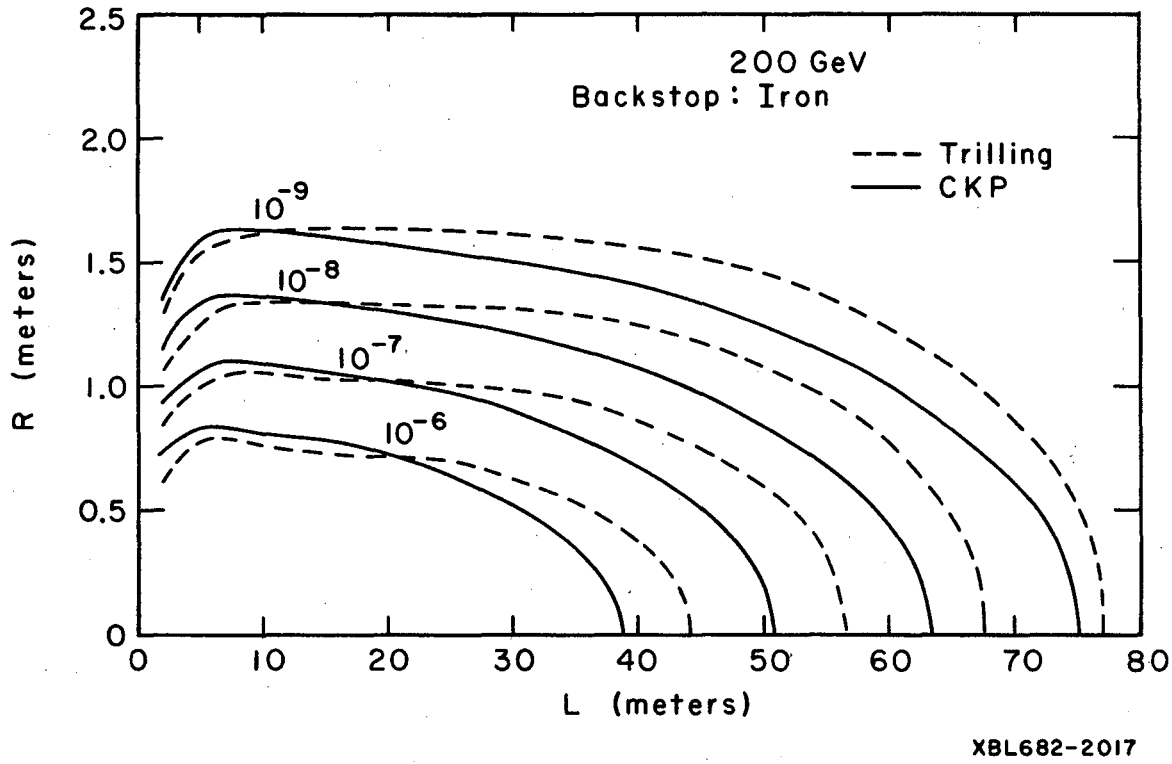
200 GeV
Backstop : Iron
Trilling
CKP
$10^{-9}$
$10^{-8}$
$10^{-7}$
$10^{-6}$
R (meters)
L (meters)
0
0.5
1.0
1.5
2.0
2.5
0
10
20
30
40
50
60
70
80
XBL682-2017

Fig. 22

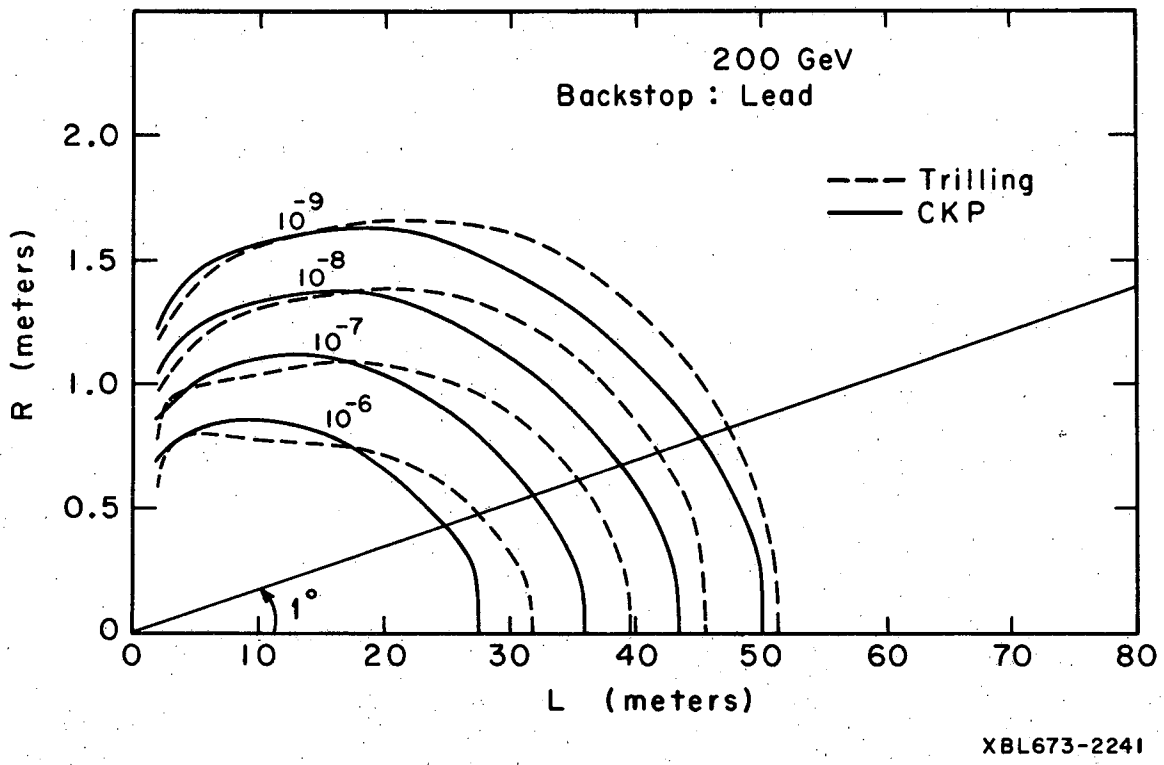
200 GeV
Backstop : Lead
Trilling
CKP
$10^{-9}$
$10^{-8}$
$10^{-7}$
$10^{-6}$
1°
R (meters)
L (meters)
0
0.5
1.0
1.5
2.0
10
20
30
40
50
60
70
80
XBL673-2241

Fig. 23

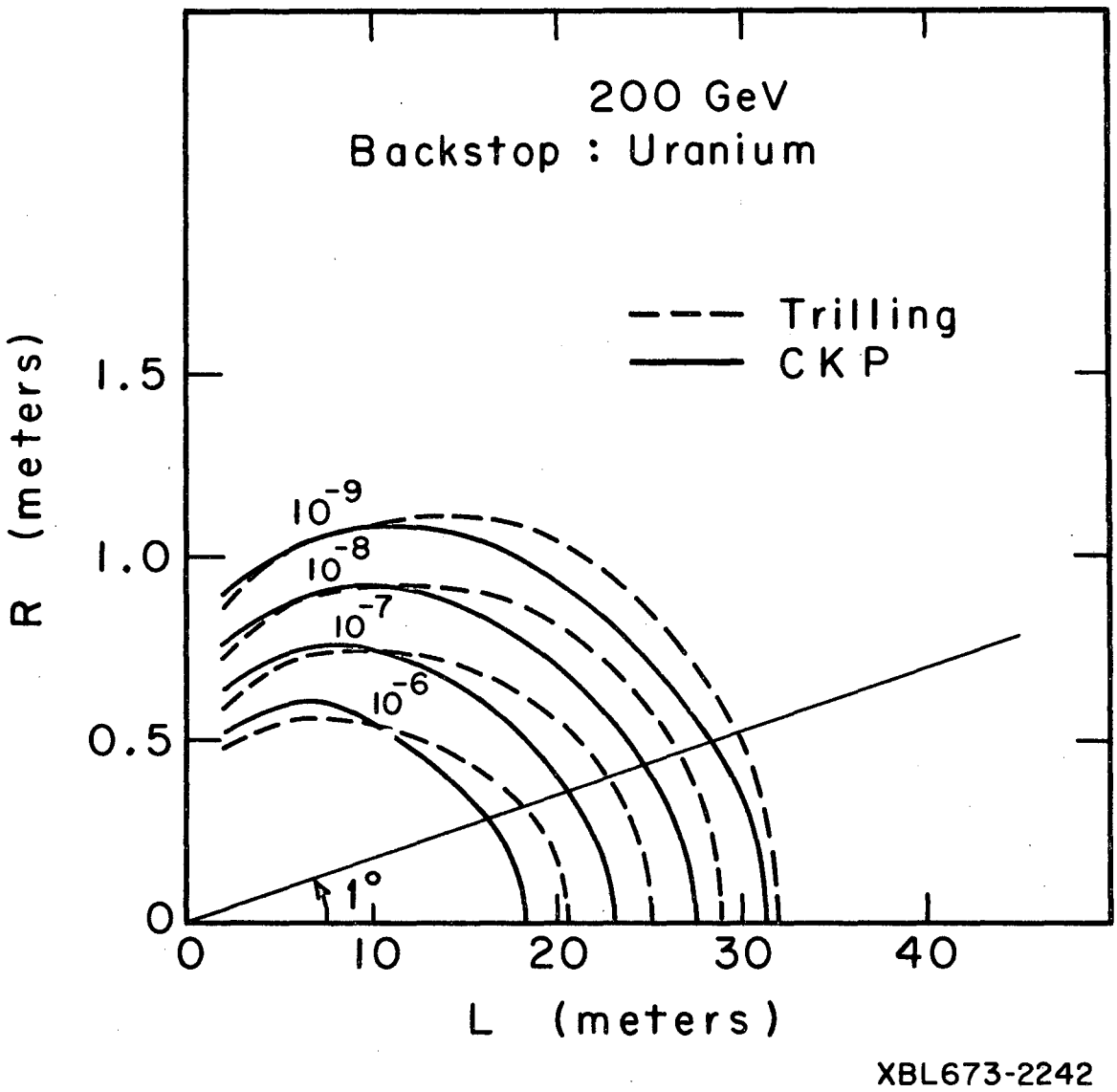
200 GeV
Backstop : Uranium
Trilling
CKP
R (meters)
1.5
1.0
0.5
0
$10^{-9}$
$10^{-8}$
$10^{-7}$
$10^{-6}$
1°
0
10
20
30
40
L (meters)
XBL673-2242

Fig. 24

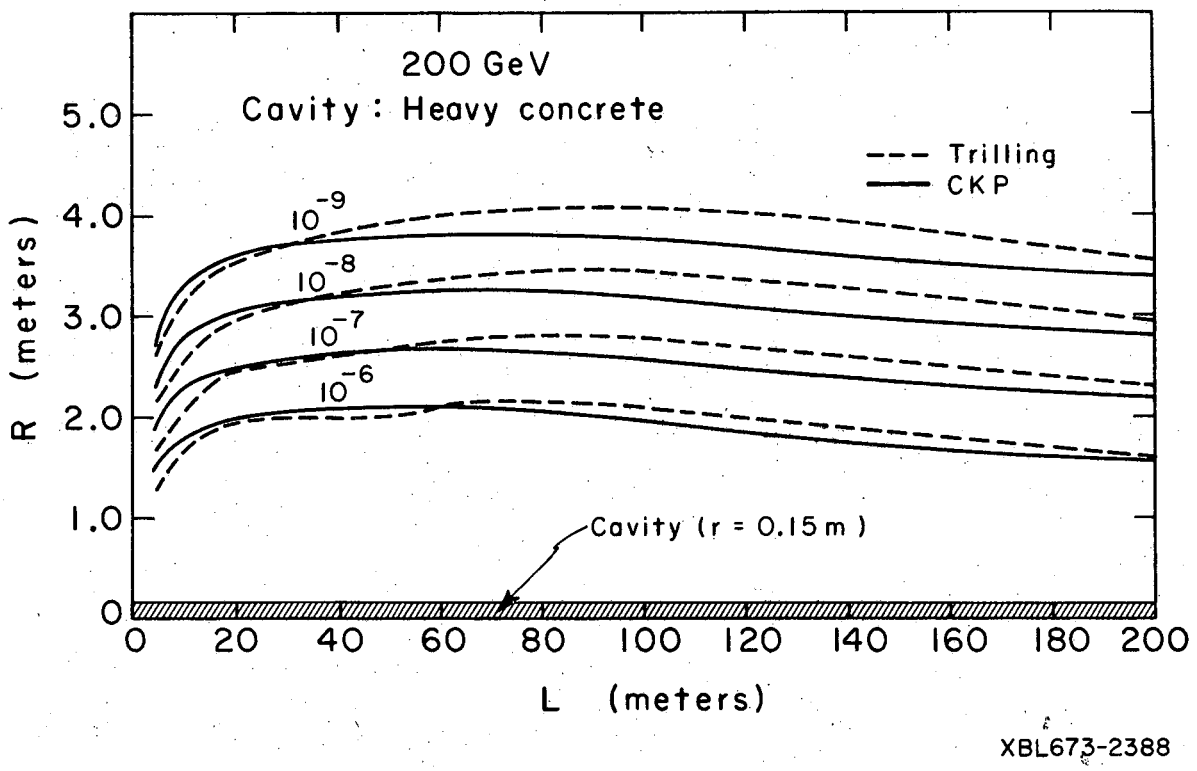
200 GeV
Cavity : Heavy concrete
Trilling
CKP
$10^{-9}$
$10^{-8}$
$10^{-7}$
$10^{-6}$
Cavity (r = 0.15 m)
R (meters)
L (meters)
0
1.0
2.0
3.0
4.0
5.0
0
20
40
60
80
100
120
140
160
180
200
XBL673-2388

Fig. 25

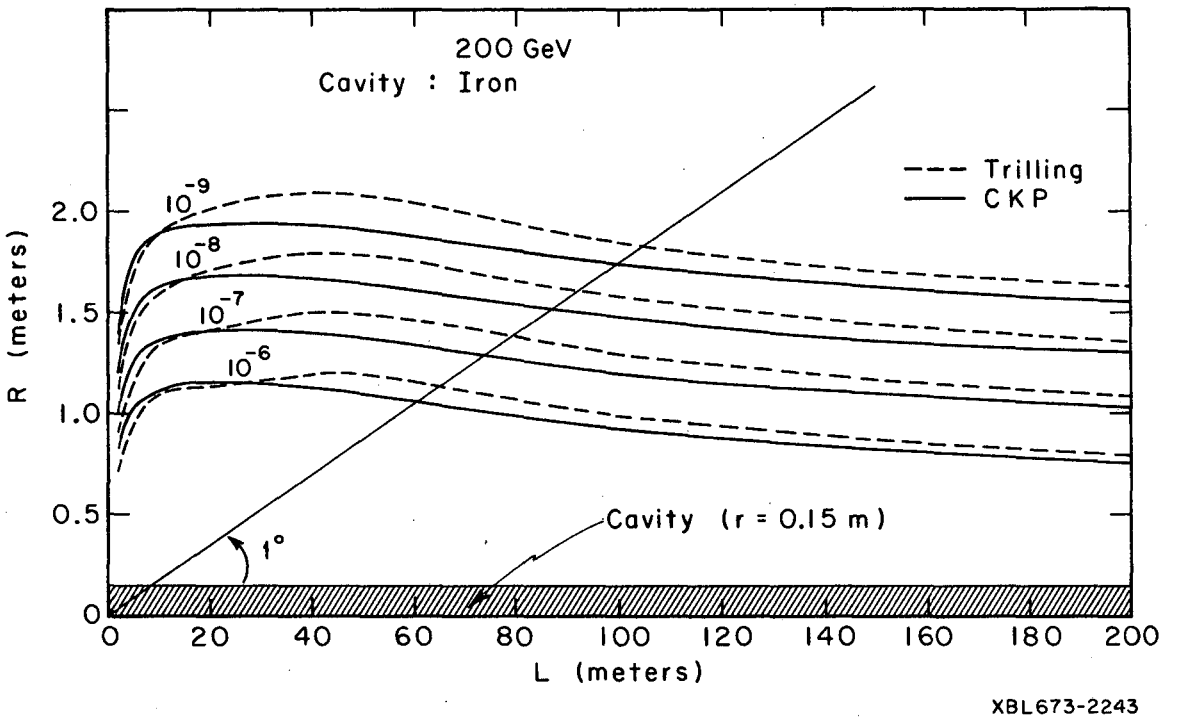
200 GeV
Cavity : Iron
Trilling
CKP
$10^{-9}$
$10^{-8}$
$10^{-7}$
$10^{-6}$
Cavity (r = 0.15 m)
1°
R (meters)
L (meters)
0
0.5
1.0
1.5
2.0
0
20
40
60
80
100
120
140
160
180
200
XBL673-2243

Fig. 26

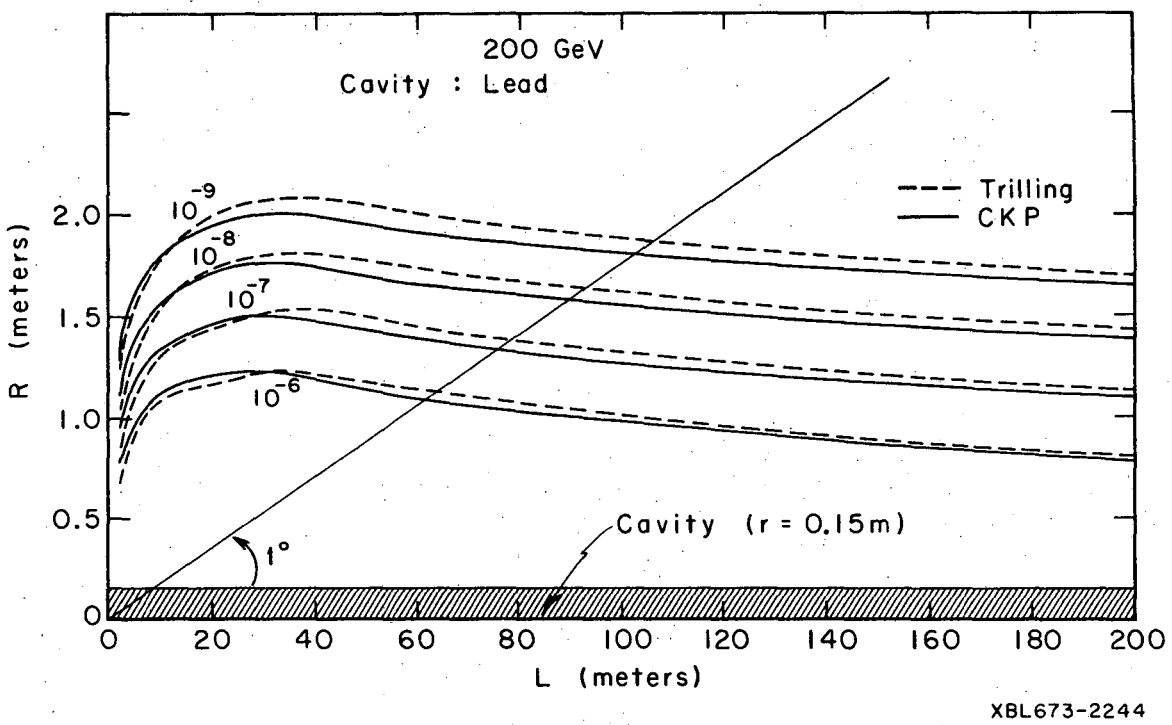
200 GeV
Cavity : Lead
Trilling
CKP
$10^{-9}$
$10^{-8}$
$10^{-7}$
$10^{-6}$
1°
Cavity (r = 0.15m)
R (meters)
L (meters)
0
0.5
1.0
1.5
2.0
0
20
40
60
80
100
120
140
160
180
200
XBL673-2244

Fig. 27

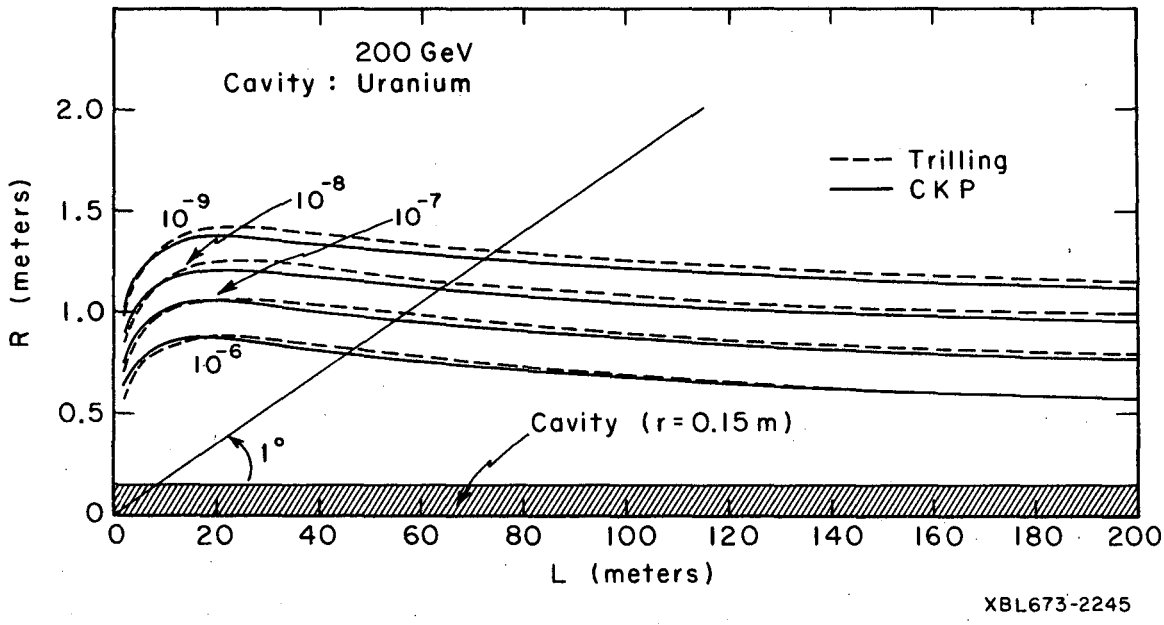
200 GeV
Cavity : Uranium
Trilling
CKP
$10^{-9}$
$10^{-8}$
$10^{-7}$
$10^{-6}$
1°
Cavity (r = 0.15 m)
R (meters)
L (meters)
0
0.5
1.0
1.5
2.0
0
20
40
60
80
100
120
140
160
180
200
XBL673-2245

Fig. 28

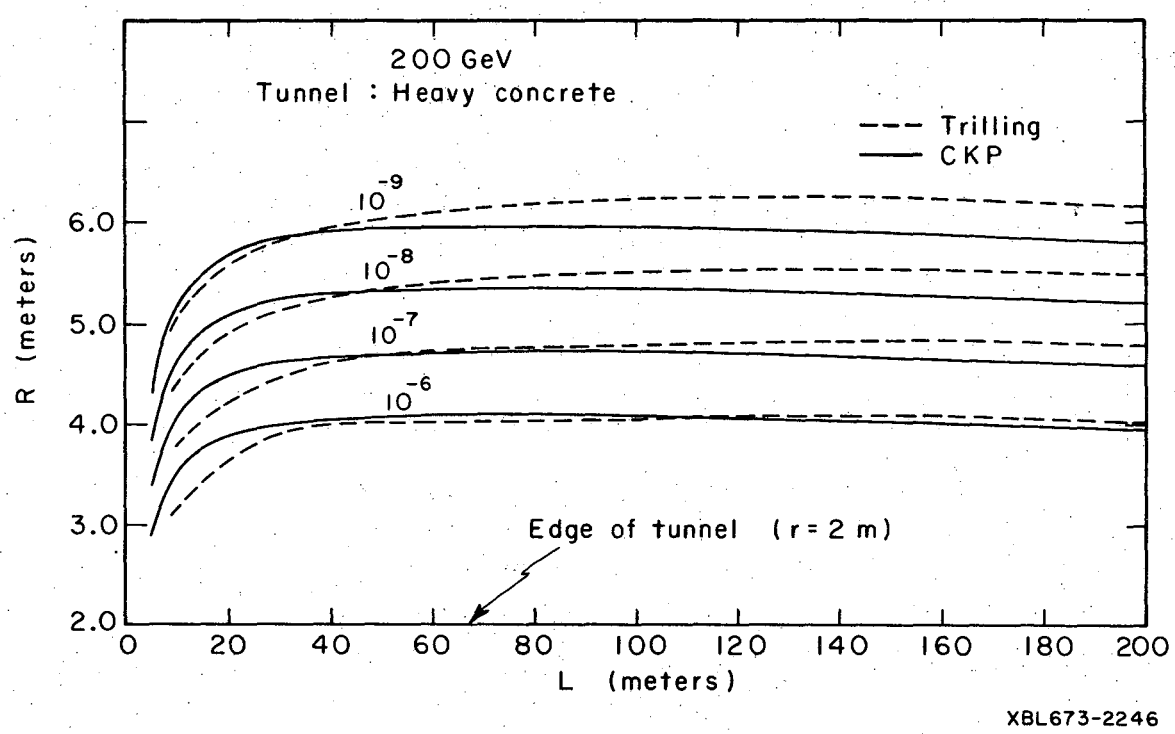
200 GeV
Tunnel : Heavy concrete
Trilling
CKP
$10^{-9}$
$10^{-8}$
$10^{-7}$
$10^{-6}$
Edge of tunnel (r = 2 m)
R (meters)
L (meters)
6.0
5.0
4.0
3.0
2.0
0
20
40
60
80
100
120
140
160
180
200
XBL673-2246

Fig. 29

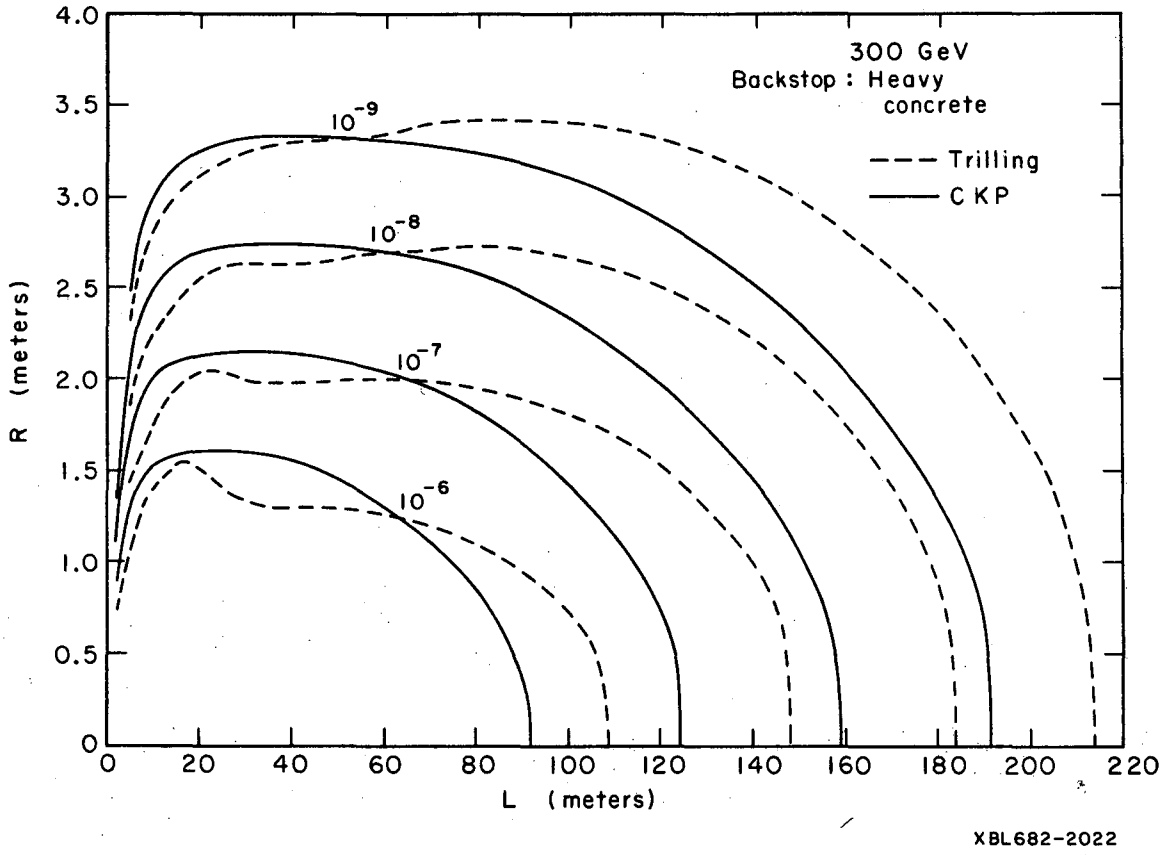
300 GeV
Backstop : Heavy concrete
Trilling
CKP
$10^{-9}$
$10^{-8}$
$10^{-7}$
$10^{-6}$
R (meters)
L (meters)
0
0.5
1.0
1.5
2.0
2.5
3.0
3.5
4.0
0
20
40
60
80
100
120
140
160
180
200
220
XBL682-2022

Fig. 30

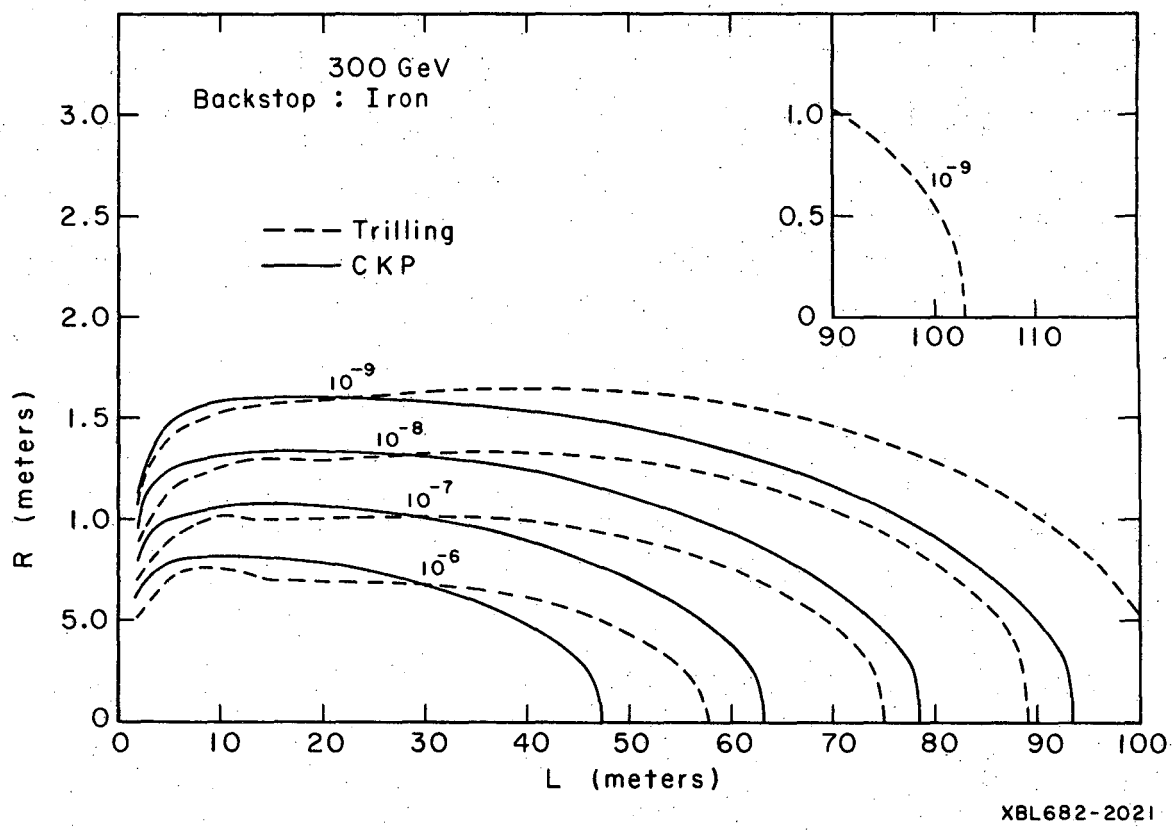
300 GeV
Backstop : Iron
Trilling
CKP
$10^{-9}$
$10^{-8}$
$10^{-7}$
$10^{-6}$
R (meters)
L (meters)
XBL682-2021

Fig. 31

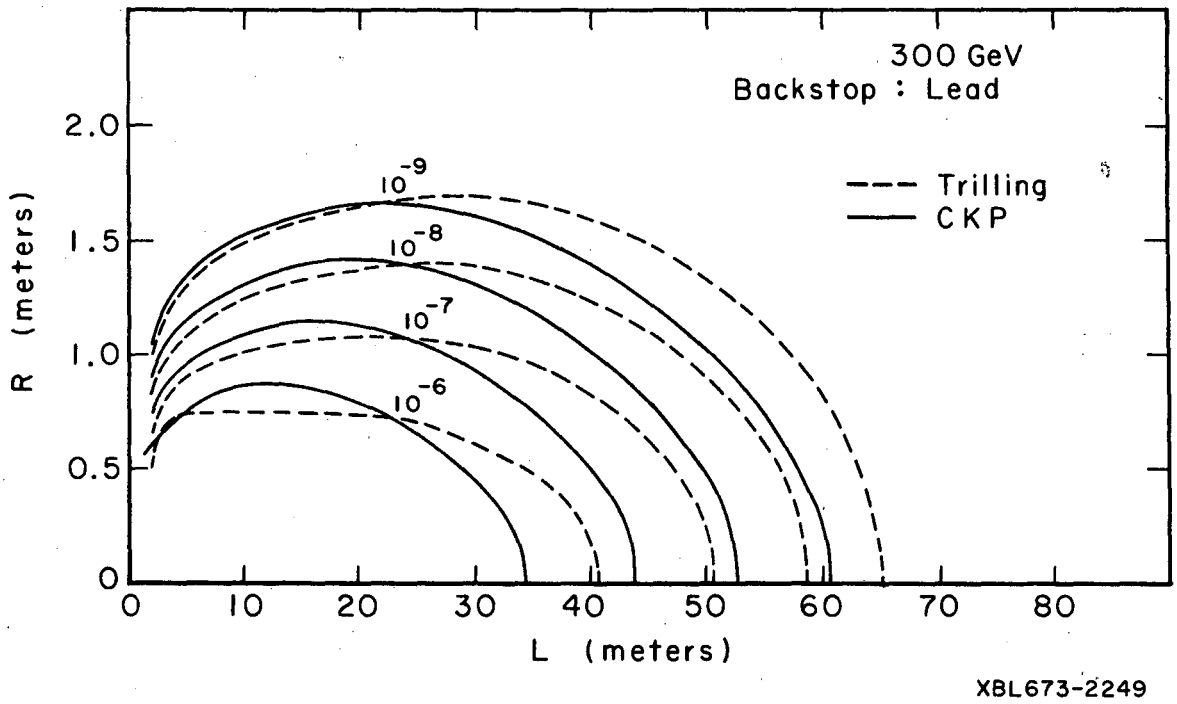
300 GeV
Backstop : Lead
Trilling
CKP
$10^{-9}$
$10^{-8}$
$10^{-7}$
$10^{-6}$
R (meters)
L (meters)
0
0.5
1.0
1.5
2.0
0
10
20
30
40
50
60
70
80
XBL673-2249

Fig. 32

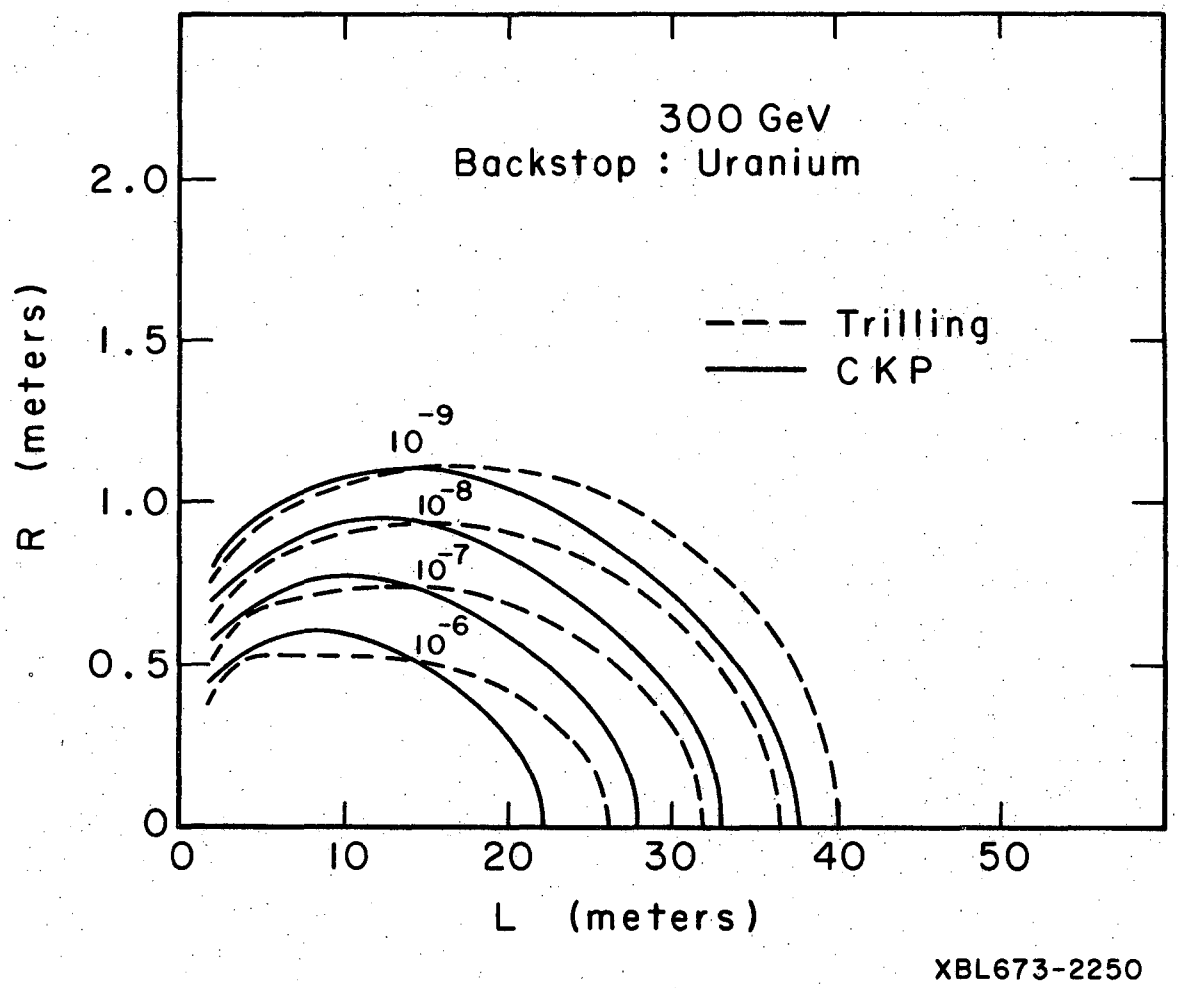
300 GeV
Backstop : Uranium
Trilling
CKP
$10^{-9}$
$10^{-8}$
$10^{-7}$
$10^{-6}$
R (meters)
L (meters)
0
0.5
1.0
1.5
2.0
0
10
20
30
40
50
XBL673-2250

Fig. 33

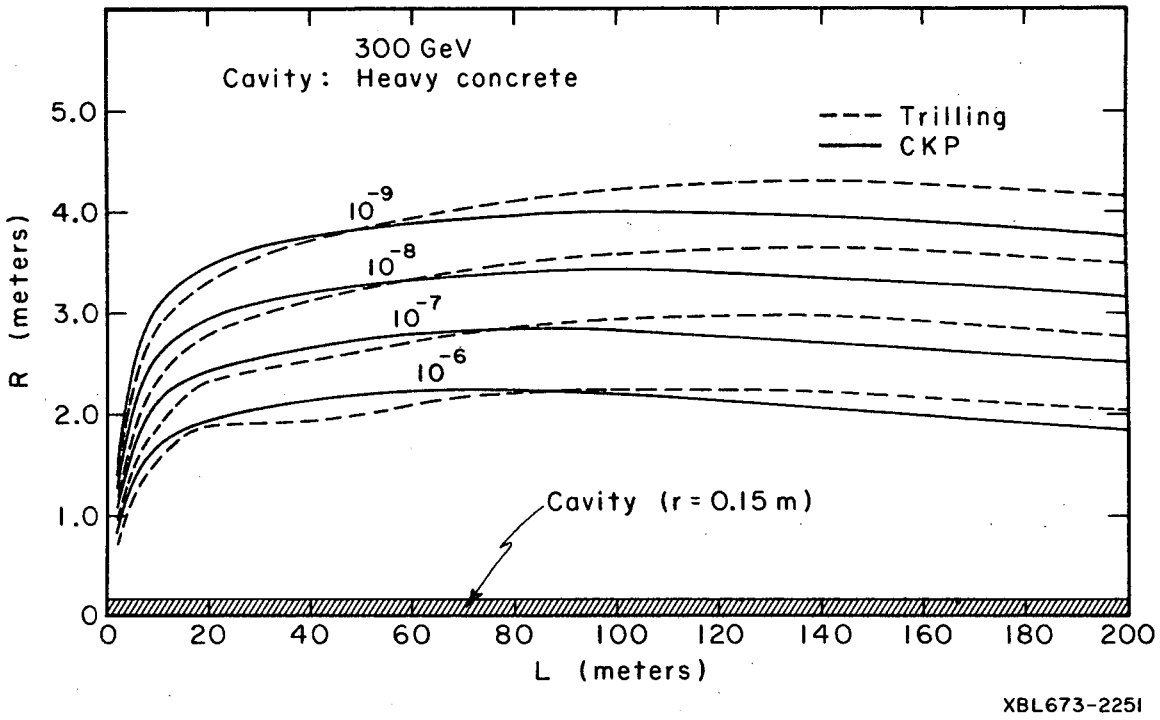
300 GeV
Cavity: Heavy concrete
Trilling
CKP
$10^{-9}$
$10^{-8}$
$10^{-7}$
$10^{-6}$
Cavity (r = 0.15 m)
R (meters)
L (meters)
0
1.0
2.0
3.0
4.0
5.0
0
20
40
60
80
100
120
140
160
180
200
XBL673-2251

Fig. 34

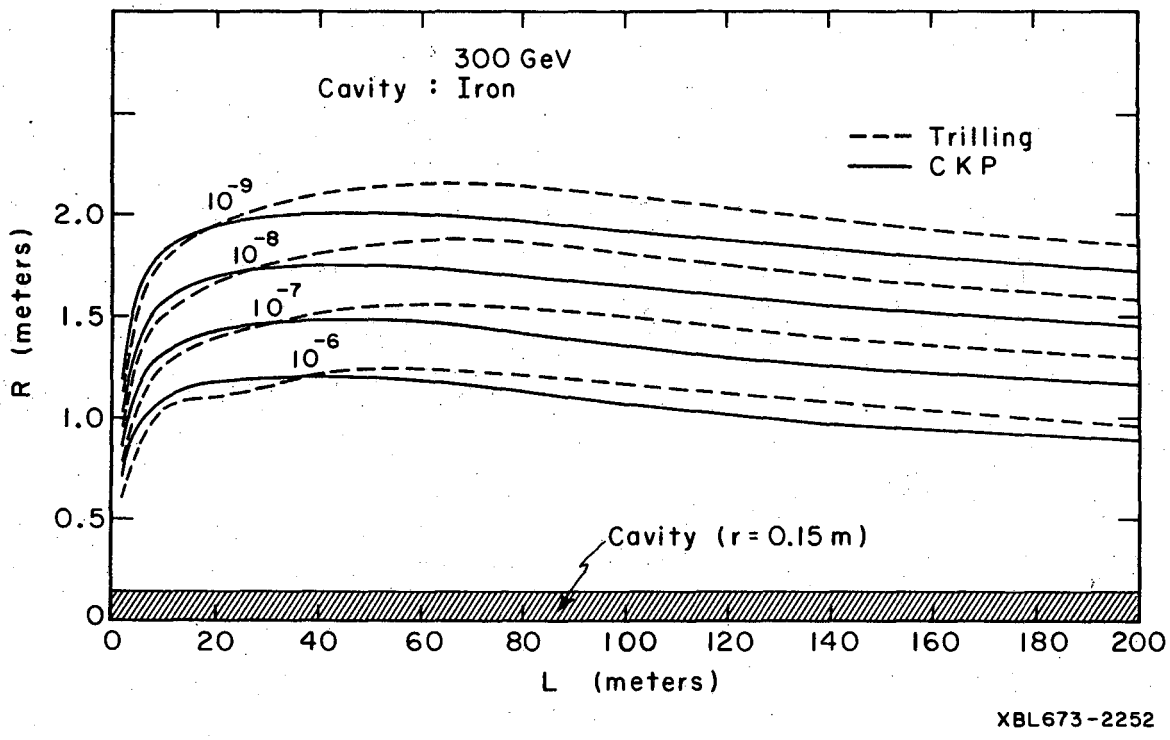
300 GeV
Cavity : Iron
Trilling
C K P
$10^{-9}$
$10^{-8}$
$10^{-7}$
$10^{-6}$
Cavity (r = 0.15 m)
R (meters)
L (meters)
0
0.5
1.0
1.5
2.0
0
20
40
60
80
100
120
140
160
180
200
XBL673-2252

Fig. 35

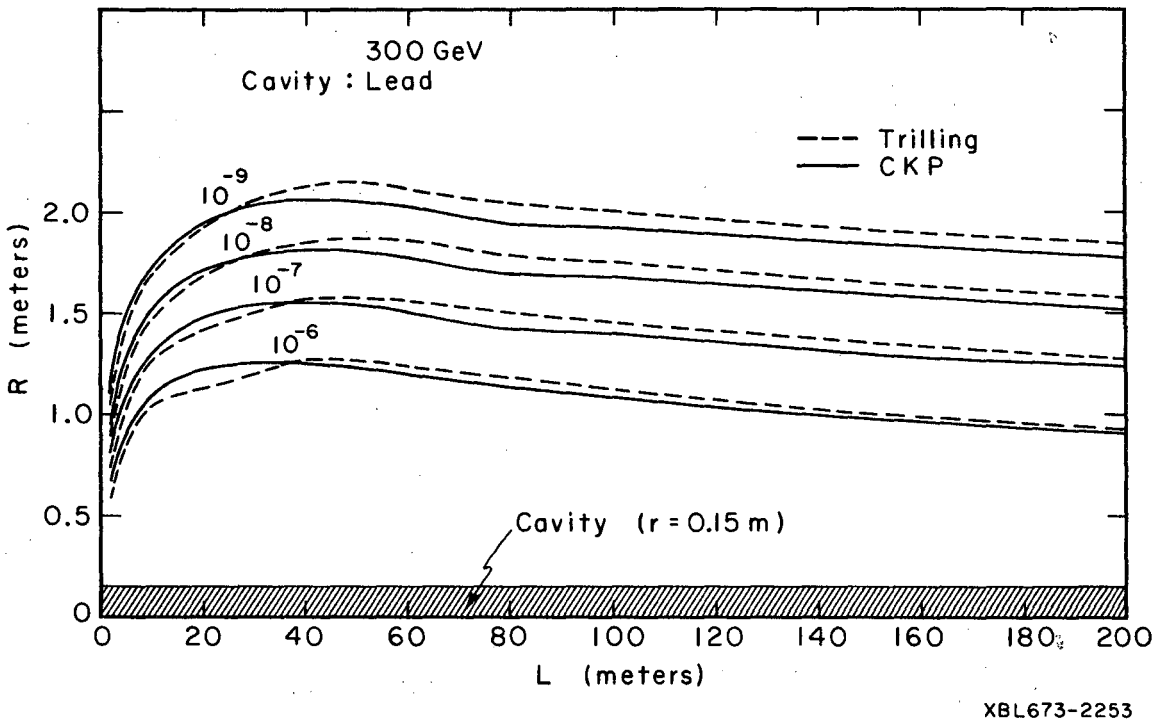
300 GeV
Cavity : Lead
Trilling
CKP
$10^{-9}$
$10^{-8}$
$10^{-7}$
$10^{-6}$
Cavity (r = 0.15 m)
R (meters)
L (meters)
0
0.5
1.0
1.5
2.0
0
20
40
60
80
100
120
140
160
180
200
XBL673-2253

Fig. 36

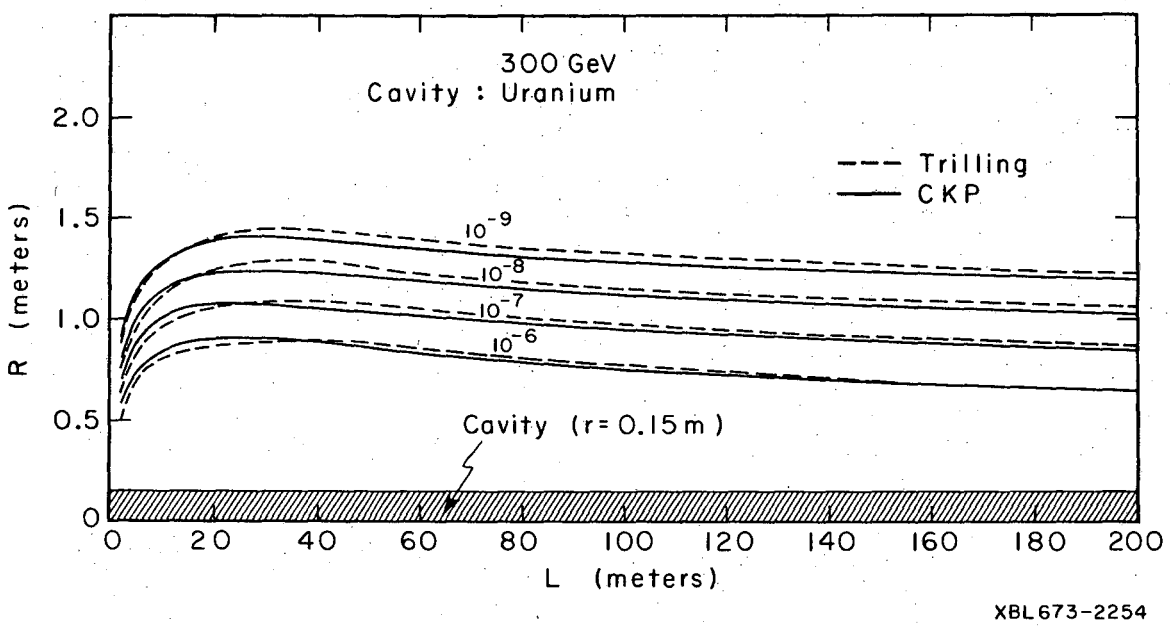
300 GeV
Cavity : Uranium
Trilling
CKP
$10^{-9}$
$10^{-8}$
$10^{-7}$
$10^{-6}$
Cavity (r = 0.15 m)
R (meters)
L (meters)
0
0.5
1.0
1.5
2.0
0
20
40
60
80
100
120
140
160
180
200
XBL673-2254

Fig. 37

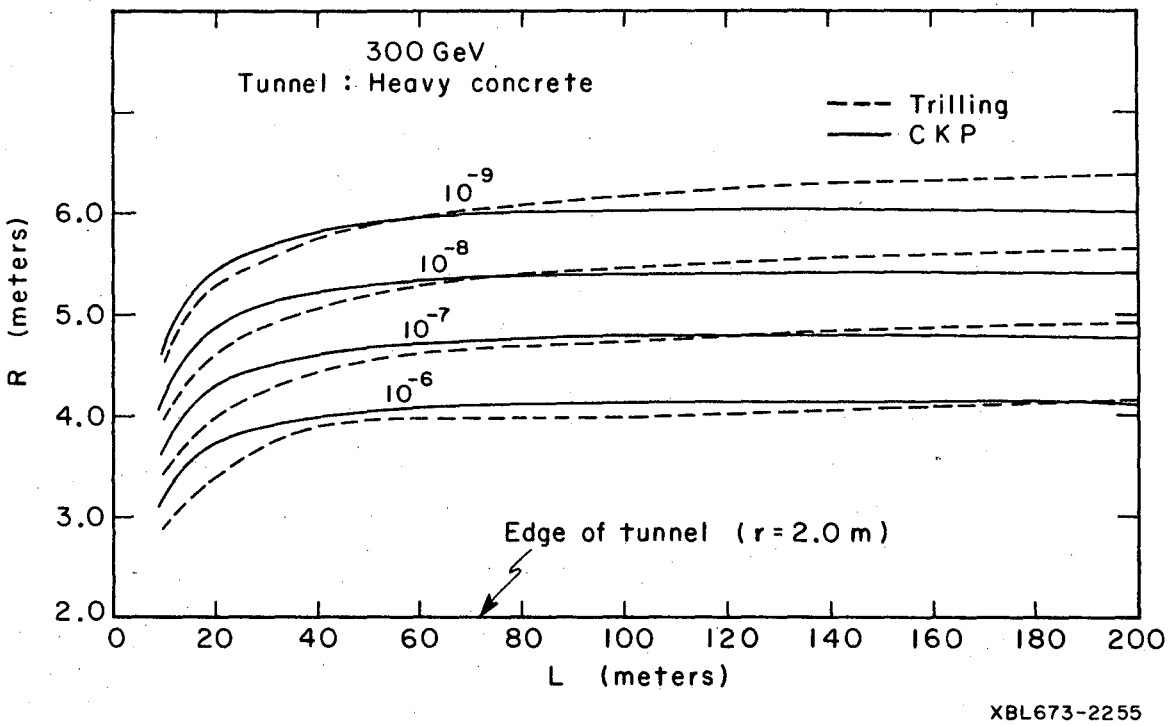
300 GeV
Tunnel : Heavy concrete
Trilling
C K P
$10^{-9}$
$10^{-8}$
$10^{-7}$
$10^{-6}$
Edge of tunnel (r = 2.0 m)
R (meters)
L (meters)
6.0
5.0
4.0
3.0
2.0
0
20
40
60
80
100
120
140
160
180
200
XBL673-2255

Fig. 38